



**AFRL-RX-WP-JA-2015-0059**

# **DYNAMIC PHOTONIC MATERIALS BASED ON LIQUID CRYSTALS (POSTPRINT)**

**Luciano De Sio and Cesare Umeton**  
**University of Calabria**

**Nelson Tabiryan**  
**Beam Engineering for Advanced Measurements Company**

**Timothy Bunning**  
**AFRL/RXA**

**Brian R. Kimball**  
**US Army Natick Soldier Research, Development & Engineering Center**

**SEPTEMBER 2013**  
**Interim Report**

**Distribution A. Approved for public release; distribution unlimited.**

*See additional restrictions described on inside pages*

**STINFO COPY**

**© 2013 Elsevier B.V.**

**AIR FORCE RESEARCH LABORATORY**  
**MATERIALS AND MANUFACTURING DIRECTORATE**  
**WRIGHT-PATTERSON AIR FORCE BASE, OH 45433-7750**  
**AIR FORCE MATERIEL COMMAND**  
**UNITED STATES AIR FORCE**

## NOTICE AND SIGNATURE PAGE

Using Government drawings, specifications, or other data included in this document for any purpose other than Government procurement does not in any way obligate the U.S. Government. The fact that the Government formulated or supplied the drawings, specifications, or other data does not license the holder or any other person or corporation; or convey any rights or permission to manufacture, use, or sell any patented invention that may relate to them.

This report was cleared for public release by the USAF 88th Air Base Wing (88 ABW) Public Affairs Office (PAO) and is available to the general public, including foreign nationals.

Copies may be obtained from the Defense Technical Information Center (DTIC)  
(<http://www.dtic.mil>).

AFRL-RX-WP-JA-2015-0059 HAS BEEN REVIEWED AND IS APPROVED FOR  
PUBLICATION IN ACCORDANCE WITH ASSIGNED DISTRIBUTION STATEMENT.

//Signature//  
TIMOTHY J. BUNNING, Chief  
Functional Materials Division  
Materials and Manufacturing Directorate

This report is published in the interest of scientific and technical information exchange, and its publication does not constitute the Government's approval or disapproval of its ideas or findings.

REPORT DOCUMENTATION PAGE				Form Approved OMB No. 074-0188	
Public reporting burden for this collection of information is estimated to average 1 hour per response, including the time for reviewing instructions, searching existing data sources, gathering and maintaining the data needed, and completing and reviewing this collection of information. Send comments regarding this burden estimate or any other aspect of this collection of information, including suggestions for reducing this burden to Defense, Washington Headquarters Services, Directorate for Information Operations and Reports, 1215 Jefferson Davis Highway, Suite 1204, Arlington, VA 22202-4302. Respondents should be aware that notwithstanding any other provision of law, no person shall be subject to any penalty for failing to comply with a collection of information if it does not display a currently valid OMB control number. PLEASE DO NOT RETURN YOUR FORM TO THE ABOVE ADDRESS.					
1. REPORT DATE (DD-MM-YYYY) September 2013		2. REPORT TYPE Interim		3. DATES COVERED (From – To) 08 June 2011 – 31 August 2013	
4. TITLE AND SUBTITLE DYNAMIC PHOTONIC MATERIALS BASED ON LIQUID CRYSTALS (POSTPRINT)				5a. CONTRACT NUMBER In-House	
				5b. GRANT NUMBER	
				5c. PROGRAM ELEMENT NUMBER 61102F	
6. AUTHOR(S) (see back)				5d. PROJECT NUMBER 3001	
				5e. TASK NUMBER	
				5f. WORK UNIT NUMBER X091	
7. PERFORMING ORGANIZATION NAME(S) AND ADDRESS(ES) (see back)				8. PERFORMING ORGANIZATION REPORT NUMBER	
9. SPONSORING / MONITORING AGENCY NAME(S) AND ADDRESS(ES) Air Force Research Laboratory Materials and Manufacturing Directorate Wright Patterson Air Force Base, OH 45433-7750 Air Force Materiel Command United States Air Force				10. SPONSOR/MONITOR'S ACRONYM(S)  AFRL/RXA	
				11. SPONSOR/MONITOR'S REPORT NUMBER(S) AFRL-RX-WP-JA-2015-0059	
12. DISTRIBUTION / AVAILABILITY STATEMENT Distribution A. Approved for public release; distribution unlimited. This report contains color.					
13. SUPPLEMENTARY NOTES PA Case Number: 88ABW-2013-2345, Clearance Date: 15 May 2013. Journal article published in Progress in Optics, Volume 58. © 2013 Elsevier B.V.. The U.S. Government is joint author of the work and has the right to use, modify, reproduce, release, perform, display or disclose the work. The final publication is available at <a href="http://dx.doi.org/10.1016/B978-0-444-62644-8.00001-7">http://dx.doi.org/10.1016/B978-0-444-62644-8.00001-7</a> .					
14. ABSTRACT Liquid crystals, combining optical non-linearity and self-organizing properties with fluidity, and being responsive to a wide variety of stimuli, have reached a key point in their development for photonic applications, for the realization of devices that could be dynamically reconfigurable, widely tunable and ultra-fast controlled. In this framework, ranging from Holography to Plasmonics, we review our recent efforts on developing a new generation of dynamic, tunable, electro- and all-optical photonic systems.					
15. SUBJECT TERMS liquid crystal, cholesteric liquid crystals, advanced materials					
16. SECURITY CLASSIFICATION OF:			17. LIMITATION OF ABSTRACT  SAR	18. NUMBER OF PAGES  68	19a. NAME OF RESPONSIBLE PERSON (Monitor) Timothy J. Bunning
a. REPORT Unclassified	b. ABSTRACT Unclassified	c. THIS PAGE Unclassified			19b. TELEPHONE NUMBER (include area code) (937) 255-6573

## REPORT DOCUMENTATION PAGE Cont'd

### 6. AUTHOR(S)

Luciano De Sio and Cesare Umeton - Department of Physics and Centre of Excellence for the Study of Innovative Functional Materials CEMIF-CAL, University of Calabria, Institute for Chemical Physics Processes IPCF-CNR

Nelson Tabiryan - Beam Engineering for Advanced Measurements Company

Timothy Bunning - Materials and Manufacturing Directorate, Air Force Research Laboratory, Functional Materials Division

Brian R. Kimball - US Army Natick Soldier Research, Development & Engineering Center

### 7. PERFORMING ORGANIZATION NAME(S) AND ADDRESS(ES)

Department of Physics and Centre of Excellence for the Study of Innovative Functional Materials  
CEMIF-CAL  
University of Calabria  
Institute for Chemical Physics Processes IPCF-CNR, UOS Cosenza  
87036 Arcavacata di Rende, Italy

Beam Engineering for Advanced Measurements Company  
Winter Park, FL 32789

AFRL/RXA  
Air Force Research Laboratory  
Materials and Manufacturing Directorate  
Wright-Patterson Air Force Base, OH 45433-7750

US Army Natick Soldier Research  
Development & Engineering Center  
Kansas Street  
Natick, MA 01760-5020



# Dynamic Photonic Materials Based on Liquid Crystals

Luciano De Sio<sup>\*</sup>, Nelson Tabiryan<sup>†</sup>, Timothy Bunning<sup>‡</sup>,  
Brian R. Kimball<sup>§</sup>, and Cesare Umeton<sup>\*</sup>

<sup>\*</sup>Department of Physics and Centre of Excellence for the Study of Innovative Functional Materials CEMIF-CAL, University of Calabria, Institute for Chemical Physics Processes IPCF-CNR, UOS Cosenza, 87036 Arcavacata di Rende, Italy

<sup>†</sup>Beam Engineering for Advanced Measurements Company, Winter Park, FL 32789, USA

<sup>‡</sup>Air Force Research Laboratory, Wright-Patterson Air Force Base, OH 45433-7707, USA

<sup>§</sup>US Army Natick Soldier Research, Development & Engineering Center, Kansas Street, Natick, MA 01760-5020, USA

## Contents

1. Introduction	2
2. Photonic Devices Based on Cholesteric Liquid Crystals	3
2.1 Electro-Responsive CLCs	3
2.2 Azobenzene LCs	12
2.3 Phototunable CLCs	15
3. Holographic Polymer Dispersed in Liquid Crystals	17
4. POLICRYPS Structures	27
4.1 Realization and Theoretical Model	27
4.1.1 <i>Fabrication Recipes</i>	28
4.1.2 <i>Theoretical Model for Composite Structures Formation</i>	29
4.2 Applications of NLC-Based POLICRYPS	32
4.2.1 <i>Switchable Holographic Grating</i>	32
4.2.2 <i>Switchable Beam-Splitter</i>	33
4.2.3 <i>Switchable Waveplate</i>	34
4.2.4 <i>Tunable Bragg Filter</i>	37
4.3 Applications POLICRYPS Based on CLC and FLC	40
4.3.1 <i>Microlaser Array</i>	40
4.3.2 <i>CLC in ULH Configuration</i>	42
4.3.3 <i>SSFLC Switching</i>	43
5. Tunable Diffractive Waveplates	45
5.1 The New Generation of Optics	45
5.2 Light Modulation Concepts Based on DWs	47
6. Liquid Crystals Active Plasmonic Nanomaterials	49
6.1 General Overview	49
6.2 Periodic Structures Hosting Plasmonic CLCs	50

6.3 Random Distribution of GNPs Layered with NLC	54
7. Conclusions	59
Acknowledgments	59
References	59



## 1. INTRODUCTION

Optics and photonics involve material sciences and device technology, at the basis of displays, computing devices, optical fibers, precision manufacturing, enhanced defense capabilities, and a plethora of medical diagnostics tools. Opportunities arising from optics and photonics offer the potential for an even greater social impact in the next few decades, related to solar power generation, efficient lighting, and faster internet. Continuously increasing data capacity requirements in telecommunications and in the next-generation of dynamically reconfigurable networks increases demand for highly compact, non-mechanical, and high speed optical devices. New materials exhibiting enhanced optical properties are key to these developments. In particular, liquid crystals (LCs) have attracted a great deal of attention in the last three decades. This is due to their capability both to behave as smart anisotropic materials, exhibiting self-organizing properties along with fluidity, and to fulfill conditions imposed from outside, due to their responsiveness to a wide variety of external perturbations, like AC, DC, and optical fields (Gennes & Prost, 1995). Indeed, the large birefringence ( $\sim 0.5$ ) of LCs allows for the realization of tunable photonic devices for both optical communications and optical sensing systems. LCs and polymers have become an exciting field of research with practical applications in flat panel displays and active optical devices. Thanks to achievements obtained in the micro/nano fabrication processes, such as Intensity and Polarization Holography, Electron Beam (E-Beam) Lithography, Focused Ion Beam (FIB), and Dip-Pen nanolithography, several composite photonic structures exploiting LCs properties have been realized. Liquid Crystals are currently playing a significant role in nanoscience and nanotechnology, too. They can be utilized as bridge between “hard matter” and “soft matter,” due to the fact that nano-structured materials do not induce significant distortions of LC phases. Various nanomaterials have been dispersed and studied in LCs to enhance their physical properties. Furthermore, alignment and self-assembly of nanoparticles themselves can be achieved inside the LC, since it acts as a tunable solvent for the dispersion of nanomaterials. As an anisotropic medium, it provides a support for the self-assembly of those materials into large organized structures, even

in multiple dimensions. Most importantly, in order to exploit the distinctive characteristics and capabilities of LC technologies, a variety of means for alignment and confinement of LCs have been investigated and employed. In this chapter, we review our achievements in the fabrication and characterization of LC-based photonic devices, underlining, in particular, the “active way” we utilize to control their properties. The most important aspects and novelties are highlighted in different sections of the paper. We begin with an overview of electro-responsive and light sensitive chiral nematic LCs. We continue by reporting on the optical and electro-optical properties of holographic structures containing several kinds of LC phases and, finally, we show how it is possible to exploit and control the plasmonic nanomaterial properties by means of LCs utilized as active host media.



## 2. PHOTONIC DEVICES BASED ON CHOLESTERIC LIQUID CRYSTALS

### 2.1 Electro-Responsive CLCs

In Cholesteric Liquid Crystals (CLCs), also called chiral nematic LCs, the molecules are arranged in a helical structure such that in each plane of the system the directors are aligned (and lay in that plane) and the director orientation changes progressively along the direction perpendicular to the planes (such direction,  $\mathbf{h}$ , constitutes the axis of the helix). If the helix axis is along  $\mathbf{z}$  and  $\mathbf{n}$  is the director orientation, the angle  $\theta$  between  $\mathbf{n}$  and a reference direction in the  $xy$  plane can be expressed as follows:

$$\theta = (2\pi/P)z, \quad (1.1)$$

where the parameter  $P$  is the pitch of the helix, that is the distance along  $\mathbf{h}$  over which the orientation of the molecules rotates by  $2\pi$ . In each  $xy$  plane (constant  $z$ ) the system only has orientational order but no translational order. Because of the periodicity in the director orientation in  $\mathbf{z}$ , CLCs behave as one-dimensional photonic bandgap system and propagation of light of certain wavelengths and polarizations states is forbidden (Blinov, 1983; Yeh & Gu, 1999). In particular, for a CLC system in a planar state ( $\mathbf{h} \parallel \mathbf{z}$ , perpendicular to the plane of the cell,  $xy$ ) and at normal incidence ( $\mathbf{k} \parallel \mathbf{e}_z$ , where  $\mathbf{k}$  is the propagation wavevector of the light beam), circularly polarized light of wavelength between  $n_o P$  and  $n_e P$  ( $n_o$  and  $n_e$  are the ordinary and extraordinary refractive indices of the material, respectively) with the same handedness as the helix is reflected by the CLC layer, while the opposite sense of circular polarization propagates through the CLC

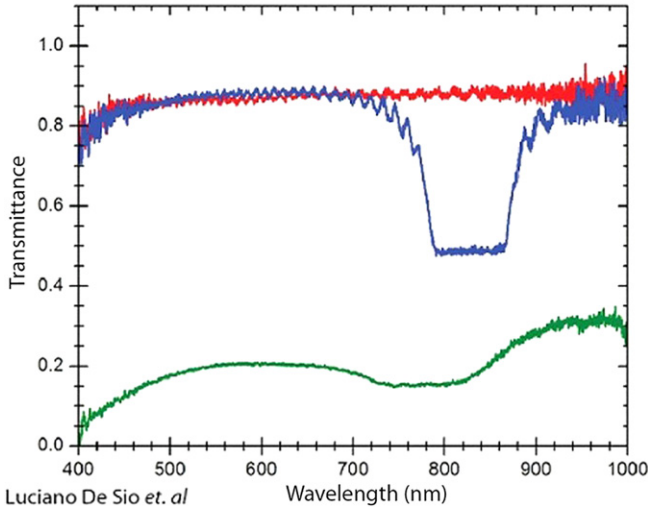


**Figure 1** Transmission spectrum of a CLC cell (80% E7, 20% R811) at normal incidence: sample in the planar homogeneous state with  $\lambda_0 = 825$  nm, no field applied (blue line); sample in a focal conic state at  $E = 1.5$  V/ $\mu$ m (green line); sample in the homeotropic state at  $E = 5$  V/ $\mu$ m (red line). All field square waves at 1 kHz. (For interpretation of the references to color in this figure legend, the reader is referred to the web version of this book.)

unaffected. For unpolarized light, an ideal sample reflects 50% of the light and transmits the remaining 50% in the wavelength range  $n_o P < \lambda < n_e P$ , whereas the sample is transparent outside this range (Figure 1, blue line). The center of the reflection band occurs at:

$$\lambda_0 = \langle n \rangle P, \quad (1.2)$$

where  $\langle n \rangle$  is the average refractive index,  $\langle n \rangle = (n_e + n_o)/2$  and the bandwidth is given by:

$$\Delta\lambda = \Delta n P = (n_e - n_o) P. \quad (1.3)$$

Because of the dielectric anisotropy of the material, the director orientation of the liquid crystals can change in the presence of an electric field, and this effect has been used to design various types of electro-responsive devices based on CLCs. For a CLC with a positive dielectric anisotropy ( $\Delta\epsilon > 0$ ), the helical structure is not stable when an electric field is applied parallel to the helical axis ( $\mathbf{E} \parallel \mathbf{h}$ ) (Blinov, 1983). When an electric field is first applied to a planar aligned (homogeneous) CLC cell, the sample becomes scattering at a field above a critical value. The axis of the helix becomes tilted (from



the original normal condition) and the sample assumes a multi-domain focal conic texture (Figure 1, green line), which does not transmit light. When the field is further increased above a second critical value, the helical arrangement of the molecules is destroyed and molecules (and overall director) become aligned parallel to the field direction (perpendicular to the cell). The sample becomes transparent (Figure 1, red line) and the large change from a reflective to transparent state by field is the basis for numerous display-related applications. However, upon removal of the field, recovery of the initial reflective state can be very slow and in many cases the sample remains trapped in the disordered focal conic texture (scattering state), limiting the utility of the system for practical applications. Two major approaches have been explored to overcome this shortcoming. The first, the use of dual frequency LCs, utilizes an applied field to drive alignment in both directions enabling fast switching between the transparent and reflective conditions (Xu & Yang, 1997). In these materials, the sign of the dielectric anisotropy depends on the electric field frequency (Bücher, Klingbiel, & VanMeter, 1974; De Jeu, Geritsma, Van Zanten, & Goossens, 1972). Below a crossover frequency,  $\Delta\epsilon > 0$ , and a homogeneous cell can be switched from the planar (reflective) to the homeotropic (transparent) state. For frequencies above the crossover point,  $1\epsilon < 0$ , an applied field will reorient the LC molecules from a homeotropic (transparent) orientation back to parallel (to the plane of the cell), facilitating the restoration of the standing helical structure. Thus, toggling between frequencies, with an applied field in both cases, will enable switching between the reflective and transparent states. Switch-off times on the order of 100 ms have been achieved using this type of material (Xu & Yang, 1997). Dual frequency CLCs have also been used to fabricate fast-switchable devices that operate between the reflective and scattering states (Gerber, 1984; Hsiao, Tang, & Lee, 2011). The shortfalls to this approach are specialty materials whose electro-optical properties are very sensitive to temperature and complex drive schemes. The second approach for increasing speed has been incorporating a loose polymer network within the CLC cells. Shortening of the recovery time by several orders of magnitude has been demonstrated (Beckel, Natarajan, Tondiglia, Sutherland, & Bunning, 2007; Hikmet, 1998; Sathaye, Dupont, & de Bougrenet de la Tocnaye, 2012). Typically, the cell is fabricated with a mixture of photopolymerizable monomers which are then polymerized using light after initial fabrication of a specific cell design (typically planar homogeneous). These systems are generally referred to as polymer-stabilized CLCs (PSCLCs). Figure 2 shows the transmission spectrum as a function of applied voltage for a PSCLC reported by Hikmet

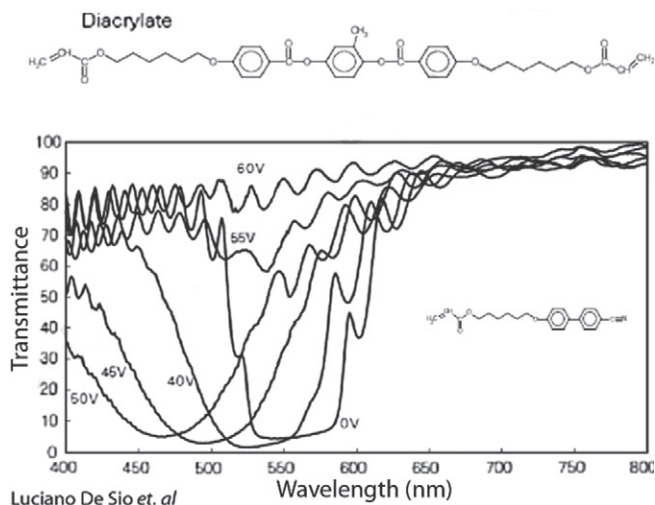


**Figure 2** Transmission spectra as a function of applied voltage for a PSCLC system containing the monoacrylate monomer shown in the inset and a small amount of diacrylate shown above the spectra. *Reproduced from Hikmet and Kemperman (1998).*

and Kemperman (1998), which was fabricated using UV irradiation. The dip in the transmission spectrum (corresponding to the reflection band of the CLC system) initially shifts to shorter wavelength when a voltage of 40–50 V is applied (the blue-shift is due to tilting of the helix axis), but the system is still highly transparent in the rest of the spectrum. At 60 V, the sample is brought into a homeotropic state and becomes transparent. Because of the presence of the polymer network, the planar homogeneous configuration can be fully recovered upon removal of voltage with switching-off times as short as a few ms (Beckel et al., 2007; Hikmet & Kemperman, 1998). The recovery time depends on the pitch and elastic constant of the liquid crystal as well as on the content of diacrylate monomer in the initial mixture. Quicker response times are typically observed for larger contents of diacrylate monomers and thus higher crosslinking density (Beckel et al., 2007; Guillard, Sixou, Reboul, & Perichaud, 2001; Hikmet & Kemperman, 1999). The polymer network, however, cannot be too dense and rigid, otherwise the strength of the interaction between the free liquid crystal molecules and the polymer network overcomes that of the field-induced reorientation and the system is no longer switchable. One drawback is that the switch-on time and voltage for the transition from the reflective to the transparent regime are typically larger in PSCLCs than in CLCs without polymer network (Hikmet & Kemperman,

1999). Polymer stabilization has also been used to achieve broader reflection bands (Broer, Lub, & Mol, 1995; Broer, Mol, van Haaren, & Lub, 1999; Hikmet & Kemperman, 1998) and to reduce the temperature dependence of the pitch. It has also been utilized to fabricate reflective reverse-mode systems which offer a much higher contrast ratio and lower operating voltages than the typical transmissive systems (Ren & Wu, 2002).

In the cases discussed above, the pitch length and thus the position of the reflection band was determined by the composition of the CLC system and was not significantly affected by the field when  $\mathbf{E} \parallel \mathbf{h}$  (apart from a small blue-shift in the band position that can be seen in some cases at low field and corresponds to a tilt of  $\mathbf{h}$ , but not changes in the pitch itself). A wider range of applications would be accessible if the reflection band could be tuned rather than just switched reversibly in different regions of the spectrum. Phototunable changes in the helical twist power and birefringence are discussed elsewhere in this article. A few electro-responsive tuning architectures have been explored and are discussed below. The development of full color (e.g., red, green, and blue), addressable CLC reflectors to decrease the complexity of stacked red-green-blue CLC pixels for full color displays has been the major driver behind exploration of tunable CLC's. If an electric field is applied perpendicular to the helical axis ( $\mathbf{E} \perp \mathbf{h}$ ) of a CLC with a positive dielectric anisotropy ( $\Delta\epsilon > 0$ ), the helical structure is deformed and the director of the liquid crystal molecules undergoes a partial reorientation toward the field direction, resulting in an elongation of the pitch [the dependence of  $\theta$  on  $z$  is no longer described by Equation (1.1)] (Blinov, 1983; Meyer, 1968). If the CLC is in a planar homogeneous state, at normal incidence, this results in a shift of the reflection band toward longer wavelengths (Figure 3) (Li, Desai, Akins, Ventouris, & Voloschenko, 2002; Xianyu, Faris, & Crawford, 2004). In this device configuration, an electric field with the appropriate orientation (in-plane field) is often achieved using a pattern of interdigitated electrodes on one of the cell substrates. The red-shift in band position increases with an increase in field strength until the limiting value in field strength for which the helix is completely unwound (infinite pitch, homogenous alignment with  $\mathbf{n} \parallel \mathbf{E}$ ), the reflection band disappears, and the sample becomes transparent under unpolarized light (the sample is a uniaxial birefringent slab). Shifts on the order of 300 nm for systems with reflection band in the visible have been achieved based on this approach (Li et al., 2002). Relatively fast response times (on the order of ms) have been reported for this process (Li et al., 2002), even without polymer stabilization. However, depending on the target application, the use of interdigitated electrodes may pose

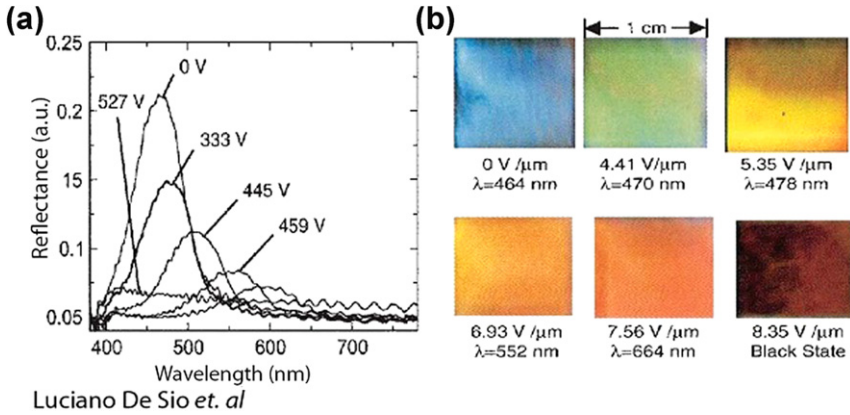


**Figure 3** (a) Reflection spectra of a CLC cell (91.5% BL118, 8.5% CB15) as a function of AC voltage (1 kHz square wave) applied in the plane of the cell. (b) Images of the same CLC cell for various applied fields (the position of the reflection band for each case is given under the image). The spacing between adjacent parallel electrodes was 64  $\mu\text{m}$ . Reproduced from *Xianyu et al. (2004)*.

limitations on the active area of the cell that exhibits the desired behavior. Additionally, because the electric field is not uniform in strength and direction in this type of cell, broadening of the reflection band and decrease in the maximum reflectance could negatively affect the performance of the tunable devices (*Xianyu et al., 2004*).

All the cases discussed above for switching and tuning devices involved CLCs with  $\Delta\epsilon > 0$  (except for the use of dual-frequency materials in devices with fast turn-off times). The response of liquid crystals with negative dielectric anisotropy ( $\Delta\epsilon < 0$ ) to an applied electric field is different. In the presence of a field, the director of a negative material tends to orient perpendicular to the field ( $\mathbf{n} \perp \mathbf{E}$ ) (*Blinov, 1983*). If the CLC system is in a planar homogeneous state ( $\mathbf{h}$  perpendicular to cell substrate), the helix conformation is stable if the electric field is directed across the cell thickness ( $\mathbf{E} \parallel \mathbf{h}$ ), as the director is already perpendicular to the field. For low frequencies, small shifts (ca. 10 nm) toward shorter wavelengths have been observed (*Lin et al., 2006*). This shift has been attributed to electrohydrodynamic effects in the cell and the segregation of space charges if the material has positive conductivity anisotropy ( $\Delta\sigma = \sigma_{\parallel} - \sigma_{\perp} > 0$ , where  $\sigma_{\parallel}$  and  $\sigma_{\perp}$  are the electrical conductivities parallel and perpendicular to the director, respectively). The field generated by the distribution of charges affects the

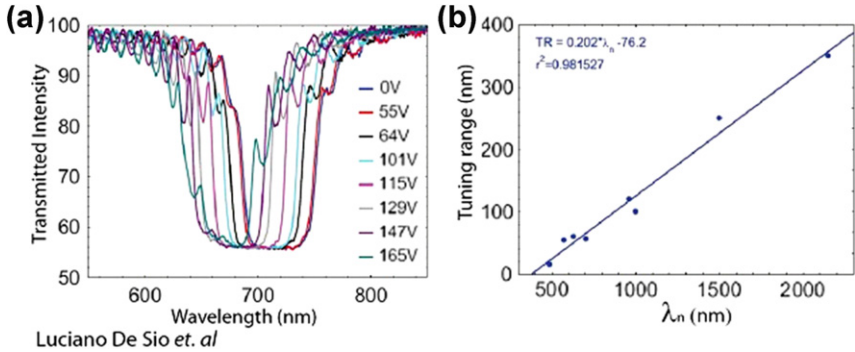


**Figure 4** (a) Transmission spectra of a CLC cell with  $\Delta\epsilon < 0$  as a function of applied DC voltage; (b) dependence of the tuning range on notch wavelength at 0 V. CLC material: 80.7% MLC-4788, 19.3% S811; cell gap = 10  $\mu\text{m}$ . Reproduced from Bailey et al. (2010).

order of the liquid crystal molecules and leads to deviations of  $\mathbf{h}$  from the original orientation and thus a blue-shift of the reflection band.

DC-field induced electromechanical effects, in particular the decrease in the cell gap due to a deformation of the cell substrates as a consequence of Maxwell stresses, was also recently shown to generate large changes ( $>300$  nm) in peak reflection wavelength as shown in Figure 4 (Bailey et al., 2010; Natarajan et al., 2008, 2007). The magnitude of the band shift depends on the cell design, the initial wavelength, and the substrate thickness. When the cell gap decreases, the material initially retains the same numbers of twists in the helix, leading to a contraction of the pitch. This effect has also been observed for AC fields when a very thin cell substrate was used (Allahverdyan & Galstian, 2011). Jumps in the location of the reflection bands have been observed at high fields (large decrease in gap), when the strain in the CLC becomes sufficiently large to overcome the surface anchoring energy (Bailey et al., 2010). The step proceeds through the formation of a transient dislocation of the director and leads to a system with a smaller number of helical twists and thus a longer pitch (Allahverdyan & Galstian, 2011). Clever cell designs can yield architectures which also red-shift the peak reflection wavelength due to an expansion in the cell gap with applied field.

A different process had been exploited by Coles and coworkers to achieve tuning to shorter wavelength of the reflection band of CLCs with  $\Delta\epsilon < 0$  and it involved the use of a Ferroelectric Liquid Crystal (FLC) (Choi, Morris, Coles, & Huck, 2007; Choi, Morris, Huck, & Coles, 2009a, 2009b). In one case, a thin layer of FLC was spin coated on the rubbed polyimide layer above the conductive substrates of the cell. When a field was applied across the

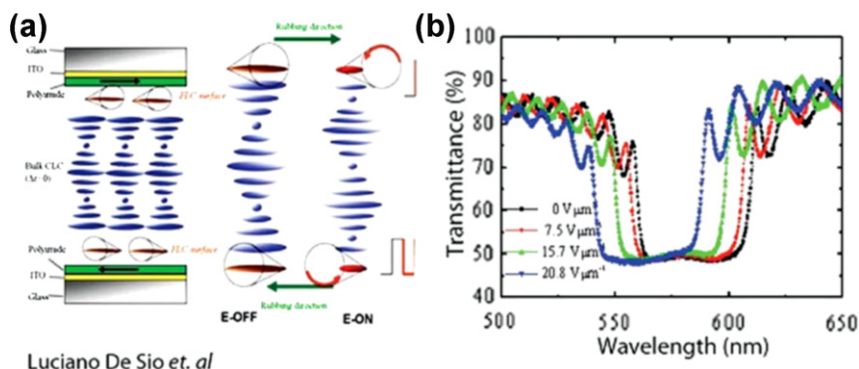
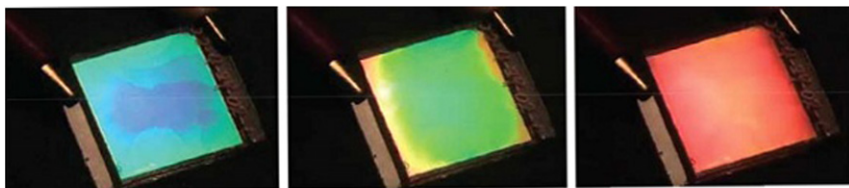


**Figure 5** (a) Schematic of CLC cell with ferroelectric surfaces and principle of operation under an AC field. (b) Transmission spectra of this type of device as a function of applied AC field across the cell (frequency = 1 kHz). CLC material: 86% MLC-7029, 10% BL006, 4% BDH1281; FLC material: R1809. Reproduced from [Choi et al. \(2007\)](#).

cell thickness, the ferroelectric layer was switched first and the electrostatic interaction between the ferroelectric layer and the chiral material near the interface resulted in a contraction of the pitch and thus a blue-shift of the reflection band ([Choi et al., 2007, 2009a](#)). A maximum shift of 23 nm was achieved with this approach (Figure 5), larger than the shift observed in the absence of the ferroelectric layer but under the same field conditions (which could be due to electrohydrodynamic effects or to helix stabilization, as discussed above) ([Choi et al., 2007](#)). In a second instance, the FLC was incorporated directly in the liquid crystal mixture filling the cell instead of being confined to the cell surfaces. Application of an AC field led again to a blue-shift in the band position as a result of the passive response of the cholesteric material to the change in orientation of the ferroelectric component ([Choi et al., 2009b](#)). The maximum shift achieved in this cell configuration was 100 nm. The times required for the band to reach a stable position after the field was turned on and the relaxation time upon removal of the field were found to be relatively slow (on the order of 100 s) ([Choi et al., 2009b](#)).

Polymer stabilization has also been explored as a tool to achieve electro-tunability of the reflection band in CLC materials. In one implementation, a cross-linkable monomer was added to the cholesteric mixture and photopolymerized to stabilize the planar texture of the CLC. A red-shift in the reflection band was induced when a voltage was applied between the top and bottom substrate of the cell ([Yu, Tang, Li, & Li, 2005](#)). Spectral shifts





Luciano De Sio *et. al*

**Figure 6** Electrically tunable device based on PSCLCs. *Image courtesy of Kent Optronics.*

of  $>500$  nm have been obtained with this approach. In this case, an AC field is utilized and the anchoring to the polymer network is strong. The field causes a tilt of the LC molecules (not the helical axis) and as a result the effective wavelength red-shifts. The reflection band becomes narrower and the peak reflection diminishes at higher wavelengths due to the smaller effective birefringence. An example of such a device in the visible range is shown in Figure 6. The electrical control of the reflection band was also used as a means to tune the lasing wavelength in polymer-stabilized CLC systems that incorporate a laser dye, as the laser emission occurs at one of the stop-band edges (Yu *et al.*, 2005).

PSCLC devices have also been produced that exhibit a blue-shift in stop band with increasing AC electric field strength (with  $\mathbf{E} \parallel \mathbf{h}$ ), but with an asymmetric behavior from the two sides of the device (Lu & Chien, 2007). When the system was illuminated from the side that was farther away from the UV light used for the polymerization, almost no reflection was observed, with and without electric field. This was attributed to the fact that the polymer network density was too low on the far side of the cell to provide sufficient stabilization to the planar texture of the CLC and the material assumed a focal conic texture. The planar texture was instead retained in the bulk of the sample and the UV-irradiation side and the material exhibited the reflection band with position and magnitude dependent on the electric field. Finally, in PSCLC systems with small dielectric anisotropy (either positive or negative), a field-dependent symmetric broadening of the reflection band has been observed for DC fields (Figure 7) (Tondiglia *et al.*, 2011). No such broadening was induced by an AC field with the material's behavior consistent with that shown in Figure 2. The broadening (up to seven times the initial bandwidth) under DC field was ascribed to a field-induced pitch distortion that is approximately linear with the depth in the cell (the pitch remaining unaltered near the center). The mechanism behind this symmetric

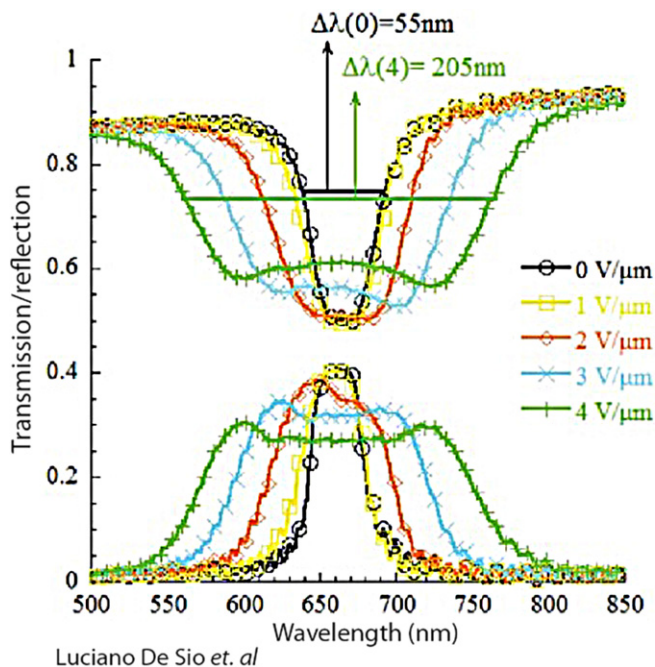


**Figure 7** Transmission (top) and reflection (bottom) spectra as a function of applied DC field in a PSCLC cell. CLC mixture: CB15 and ZLI-2079; LC monomer: RM257; initiator: Irgacure 651. Reproduced from *Tondiglia et al. (2011)*.

broadening, related to charge trapping on the polymer network coupled to field-induced polymer movement, is under exploration.

## 2.2 Azobenzene LCs

Azobenzene is a photosensitive molecule that undergoes geometrical isomerization when absorbing light (Figure 8) (*Knoll, 2004*).

The isomerization is fully reversible, and there is no limit to the number of isomerization cycles that the molecule can undergo. Change in the shape of the molecule as a result of photoisomerization can strongly influence the macroscopic material properties: optical, mechanical, rheological, transport, binding, etc. This influence is particularly significant in azo LCs due to the effect of isomerization on both the liquid crystalline order and orientation of molecules (*Anderle, Birenheide, Werner, & Wendorff, 2006; Blinov, 1996; Wendorff, 2006*). Individual photoisomerization events take place at picosecond timescales and with high quantum efficiency  $\sim 0.5$ . The  $\pi-\pi^*$  absorption band of *trans* isomers, most efficient for photoisomerization, is typically



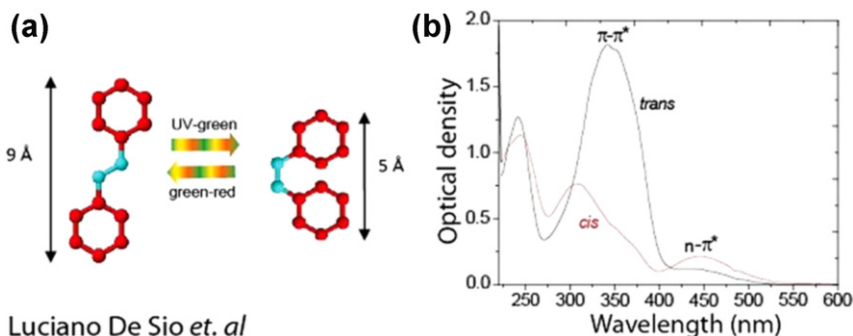


**Figure 8** Photoisomerization of azobenzene molecule (a) and absorption spectra (b) of *trans* and *cis* isomers of a room temperature azo LC 1005.

in the UV-blue region of wavelengths. *Cis* isomers are more absorptive in the green/red part of the spectrum; however, even at room temperature, they may undergo spontaneous relaxation into the *trans* state due to the relatively small energy barrier between *trans* and *cis* configurations. The peak absorption for a room temperature single component azo LC D307 (Hrozhyk, Serak, Tabiryan, & Bunning, 2006) is at 332 nm and 443 nm for *trans* and *cis* isomers with respective absorption constants  $1.25 \times 10^5 \text{ cm}^{-1}$  and  $9.6 \times 10^3 \text{ cm}^{-1}$ . The peak absorption wavelengths for azobenzene isomers can be varied by modifying their molecular structure. Peak wavelengths exceeding 575 nm have been obtained by attaching donor and acceptor groups at the opposite ends of the molecule without sacrificing mesogenic ability in some cases (Hrozhyk et al., 2008). The difference in absorption of *trans* and *cis* isomers is considerable over the entire visible spectrum. At 532 nm, a wavelength of great importance for laser technologies, the absorption constants for azo LC mixture 1005 are  $450 \text{ cm}^{-1}$  and  $1480 \text{ cm}^{-1}$  for the *trans* and *cis* isomers, respectively. In the *trans* state, azobenzene molecules are highly dichroic. The absorption constants of azo LC 1005 at 532 nm are  $840 \text{ cm}^{-1}$  and  $220 \text{ cm}^{-1}$  for polarization parallel and perpendicular to the LC optical axis, respectively. Thus photoisomerization may result in substantial changes of the absorption spectrum of azobenzene materials both due to accumulation of *cis* isomers as well as due to molecular reorientation. The effect of radiation on materials containing azobenzene moieties is essentially determined by the wavelength. Radiation of UV-wavelengths, absorbed predominantly by *trans* isomers, leads to accumulation of large concentrations of *cis* isomers. Due to comparable photoisomerization rates for both isomers, radiation of blue-green wavelengths may induce repetitive *trans*–*cis*–*trans* isomerization

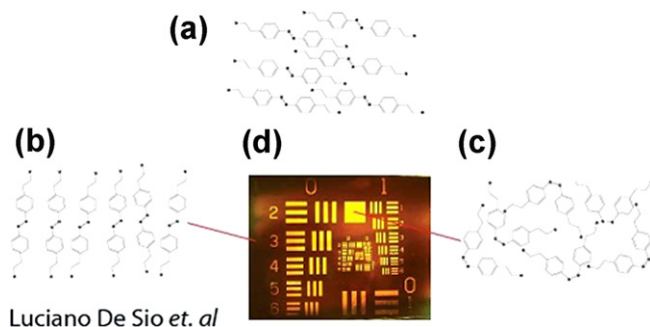


**Figure 9** Photoinduced transformations of azo LCs. A homogeneously aligned azo LC (a) undergoes reorientation with a linear polarized light of blue–green wavelengths (b) and is transformed into an isotropic phase at the effect of UV light (c). The latter can be reversed back to the mesophase with a light of visible wavelengths. (d) An optically recorded pattern of isotropic phase of LC in azo PDLC film.

cycles resulting in statistical alignment of highly dichroic *trans* isomers of azobenzene molecules perpendicular to the polarization of light (Figure 9).

The so-called photoalignment phenomenon of azobenzene is widely used for developing anisotropic thin films (Chigrinov, Kwok, Takada, & Takatsu, 2005; Ishihara, 2005). Thin azobenzene polymer films coated on glass substrates allow the orienting of LC molecules without conventional mechanical buffing. Since the polarization of light beams can be modulated with high spatial resolution, the photoalignment techniques are used for creating patterns and micropatterns of optical axis orientation in LCs and LC polymer films acting as waveplates, polarizers, and gratings. The impact of micropatterned anisotropic films extends well beyond displays with emerging applications including polarization imaging. Large area high quality diffractive waveplates (polarization gratings) produced in thin films of LCs and LC polymers ( $\sim 1\ \mu\text{m}$  for optical wavelengths) using photoalignment processes exhibit nearly 100% diffraction efficiency for the zeroth order diffraction in a broad band of wavelengths and angles. The lifetime of *cis* isomers depends on the molecular structures attached to the azobenzene core and can extend from a few milliseconds for so-called push–pull series of materials to many hours for azobenzenes with a more localized  $\pi$ -electron system. The materials with long *cis* isomer lifetimes can be used in many applications in both states, liquid crystalline (*trans*) and isotropic (*cis*). Essentially, these are two very different materials that are switched one into another by light. The photoinduced isotropic state of azo LCs can be used for various applications as “UV rechargeable” materials (Serak & Tabiryan, 2006; Tabiryan, Hrozhyk, &

Serak, 2004). Both reorientation and phase transformation processes shown in Figure 9 can take place at very low power radiation in a timescale inversely proportional to the power density. The nematic–isotropic transition time for azo LC 1005 ( $L = 0.34 \mu\text{m}$ ) is 10 s at  $14 \text{ mW}/\text{cm}^2$  power density of UV radiation ( $\lambda = 365 \text{ nm}$ ). A photoinduced phase transition can be observed in a single short UV laser pulse:  $0.56 \mu\text{m}$  thick layer of azo LC D307 is transformed into an isotropic state within 50 ns by a single pulse of 5.3 ns duration and 355 nm wavelength.

### 2.3 Phototunable CLCs

A number of electro-optical and non-linear optical materials allow producing diffractive optical components with variable characteristics. Particularly valuable are optical gratings of high diffraction efficiency obtained in thin material layers. Many of such gratings are made LCs, materials with the highest electro-optical and non-linear optical coefficients, also offering the largest modulation of refractive index. In one class of LC materials, CLCs, periodicity of optical properties is obtained due to intermolecular forces, without externally imposed processes, and it can be at the scale of visible wavelengths. The pitch of the helicoidal structure of CLCs is sensitive to all the factors capable of affecting the balance of molecular interactions and the orientation of CLC molecules. As we already discussed, the spectral characteristics, width and position, of the photonics bandgap associated with the CLC helix can be controlled by applying electric fields, changing temperature, or exposing CLCs to optical radiation. Such opportunities could not be left unnoticed. Starting from the first observations in 1970s, remarkable progress was made in producing CLC materials, both low molecular weight as well as polymer, tunable with UV radiation. A series of CLCs phototunable with radiation of visible wavelengths typical to large classes of lasers was developed and studied recently. The pitch of the CLC helix is determined by relative concentration of mesogenic trans and non-mesogenic cis isomers of azo nematic LC (NLC) molecules. Photoisomerization affects their balance, and the CLC pitch changes as a result. Two main types of phototunable CLC compositions were studied: CLCs photosensitized with azo NLCs, and azo NLCs twisted into helical structure with chiral dopants. Due to mesogenic nature of azo NLCs, the azobenzene can make up a substantial part of CLC material compositions in both cases underlying high photosensitivity of these CLCs to visible wavelengths, along with UV radiation, and large phototuning range spanning from blue to near IR parts of the spectrum (Figure 10).

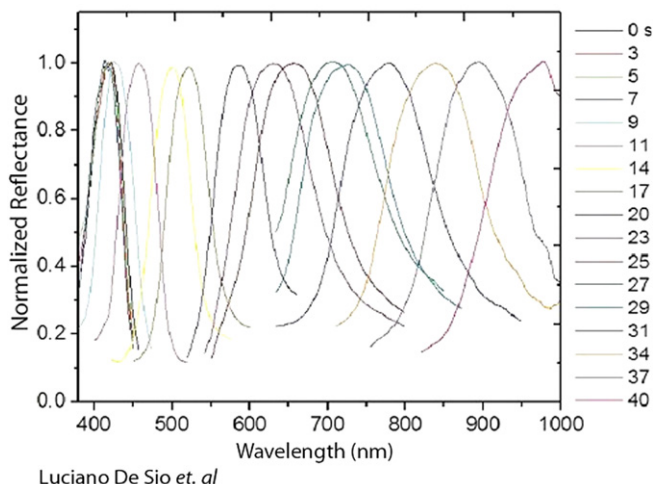


**Figure 10** Photoinduced shift in the Bragg reflection bandgap upon illumination by a violet LED ( $10 \text{ mW/cm}^2$ ) for different time periods.

Depending on the material composition, the bandgap of these CLCs can shift toward blue as well as red wavelengths under the influence of light. Propagation of a laser beam with a wavelength outside the bandgap may be blocked due to the shift of the bandgap induced by the beam itself. Such “autotuning” was demonstrated for laser beams of different wavelengths, starting from microwatt power for laser beams of 532 nm wavelength. The closer the CLC bandgap is tuned to the wavelength of the laser beam, the higher its reflection, and the smaller portion of the light reaches the bulk of the CLC. Due to such a negative feedback, the transmission of the CLC stays low in this process for over four orders of magnitude dynamic range of the incident beam power (Serak, Tabiryan, & Bunning, 2007). An important application of such phototunable bandgap materials is optically tunable lasers in a wide spectral range. Ultimately, in CLCs with large azobenzene content ( $>20 \text{ wt}\%$ ), the periodic (helical) structure can disappear due to CLC–isotropic phase transition most efficiently induced by UV radiation (Hrozhyk, Serak, Tabiryan, & Bunning, 2007). The helical structure of CLCs can be restored consequently by a laser beam of a visible wavelength. Such a bandgap switching covering a wide range of the visible spectrum was shown using a CLC material with a pitch gradient across the area of the cell (Figure 11).

Evolution times of photoinduced bandgap variations decrease with increasing power density of radiation. They are typically at 10–100 ms scale

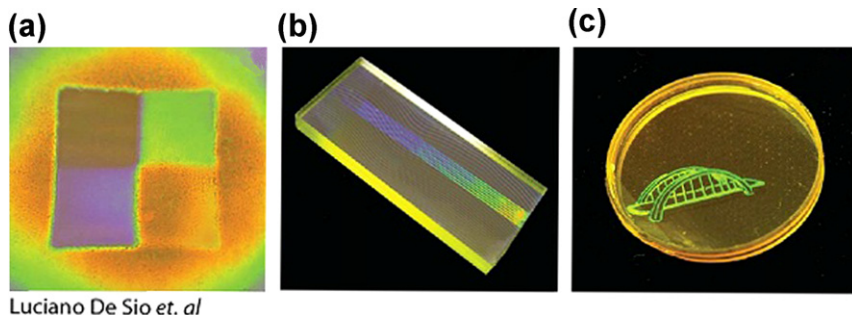


**Figure 11** (a) A color pattern recorded in CLC 1445 doped with 25 wt% of chiral azo dopant ChAD-4S (BEAM Co.) due to different UV exposure energy. (b) Restoration of the CLC bandgap gradient in the form of a grating from photoinduced isotropic state by scanning a green laser beam. (c) Selective restoration of Bragg reflective structure of a CLC doped with azo NLC 1005 from photoinduced isotropic state by scanning a focused green laser beam.

for low power CW beams, but are induced with short, nanosecond, laser pulses as well (White *et al.*, 2009).



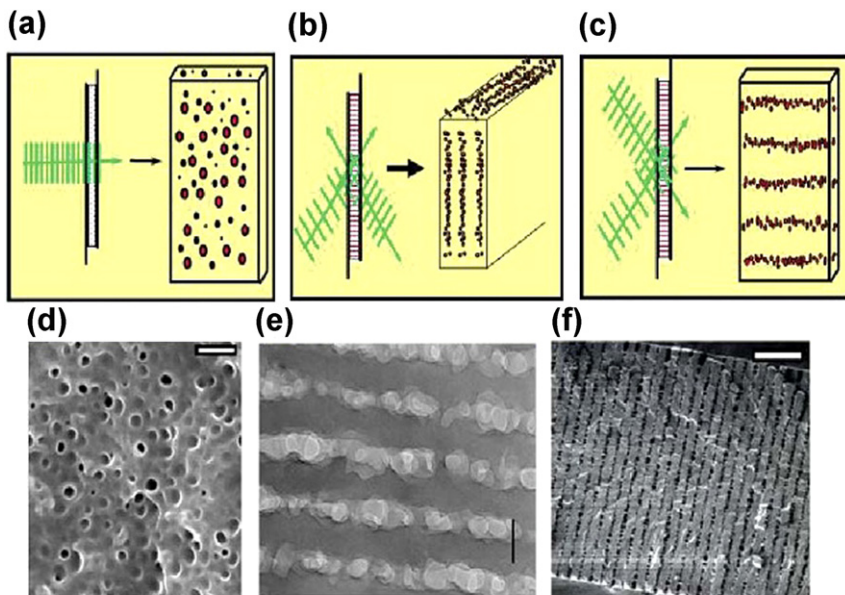
### 3. HOLOGRAPHIC POLYMER DISPERSED IN LIQUID CRYSTALS

Optical grating structures (stratified media) within a thin film possess a periodic variation of the index of refraction  $n$  and/or absorption coefficient throughout the thickness of a film. These profiles may be a smooth gradation in material properties across the period or a step-change function. Typically, the variation in refractive index is small relative to the average index across the grating. Two types of gratings, Raman–Nath or Bragg, designate the extreme cases for the film and their optical properties. Raman–Nath diffraction results from an optically thin medium (physically thin and/or low modulation amplitude) and yields a high number of diffraction orders (multiple beam diffraction) with energy distributed among all the orders. Bragg diffraction is associated with an optically thick medium (physically thick and/or high modulation amplitude) and yields a single diffraction order. When the grating structure is composed in part with a material whose optical properties can be modulated, dynamic photonic behavior is enabled. In the case of LCs materials, application of an electric field can yield dynamic grating structures whose diffracted or reflected (transmitted) optical properties can be controlled. Manufacturing these multi-functional photonic

structures whose properties can be modulated using a variety of external stimuli is of crucial importance for a myriad of optical applications where one wants to control the generation, flow, and sensing of light.

Holographic photopolymerization (HP) is a simple, fast, and attractive means to fabricate one-, two-, and three-dimensional (1D, 2D, 3D) complex structures with length scale periodicity commensurate with the optical regime. Similar to interference lithography (IL) (Campbell, Sharp, Harrison, Denning, & Turberfield, 2000), HP employs multiple light beam interference and photosensitive material mixtures to record information although there are significant differences with classic interference lithography techniques. A typical HP “recipe” contains ca. 20–50 vol.% “inert” materials that are not involved in the polymerization but whose anisotropic diffusion is critical to the successful formation of a patterned structure. The photopolymerizable syrup is first exposed to two or more coherent laser beams, the interference of which creates a standing wave pattern on a length scale dictated by the interference angle and the laser source. Higher intensity regions within the standing wave result in locally faster polymerization processes (spatially varying reaction rates), which, in turn, leads to a spatial distribution of polymer across the grating period. This process results in a segregation of reactive versus non-reactive (inert) materials via directional transport onto patterns whose length scales are dictated by the writing geometry. The nature of the photopolymerization, particularly the kinetics driven by monomer type (chain-growth versus step-growth), the length scale/kinetics of the diffusion (grating spacing), and the compatibility of the starting inert materials with both the initial reactive fluid and final polymer matrix, all factor in determining the final local “grating” morphology which in turn dictates the optical properties. These holographic structures can be fabricated within seconds and the symmetry, dimensionality, size, and refractive index modulation can be easily controlled by the fabrication conditions and starting materials. One particular advantage of using light to form these structures is that length scales of interest to structured photonic elements, hundreds of nanometers, are easily obtained.

LCs, inert from a polymerization perspective, have been extensively studied and the resulting class of structures are known as Holographic Polymer-Dispersed Liquid Crystals (HPDLCs). Several reviews exist which go into detail about the fabrication, characterization, and performance of such systems (Bunning, Natarajan, Tondiglia, & Sutherland, 2000; Crawford, 2003; Liu & Sun, 2008). The uniqueness of these structures arise from the ability to modulate the refractive index contrast of the volume holograms formed



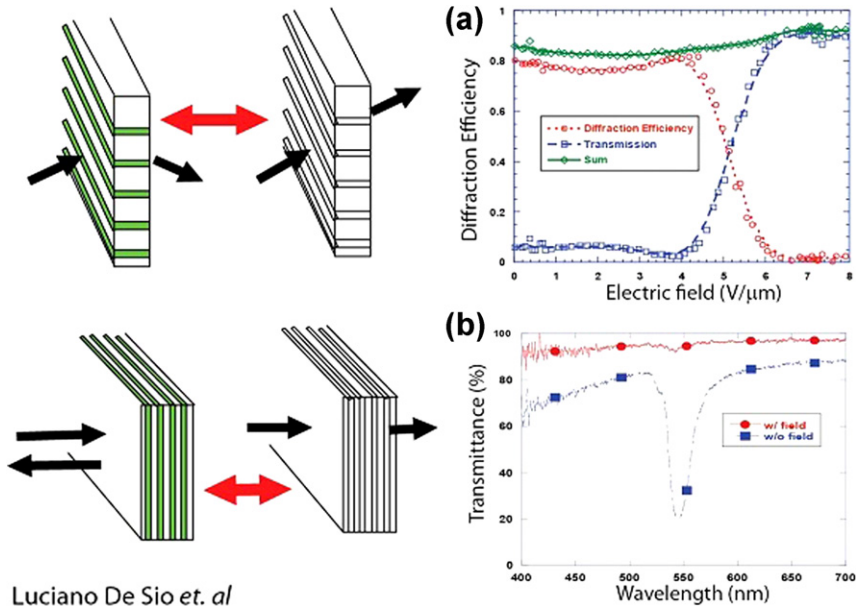
Luciano De Sio *et. al*

**Figure 12** Schematic of (a) isotropic polymer-dispersed liquid crystals, (b) reflection grating, and (c) transmission grating. (b) and (c) are formed using holographic photopolymerization. The green arrows indicate the direction of the writing beams and the small droplets represent nanoscale LC domains. (d), (e) and (f) show the corresponding Scanning Electron Microscopy (SEM) images of the cross-sections of (a), (b), and (c); scale bars are 3.75  $\mu\text{m}$ , 150 nm, and 750 nm, respectively. (For interpretation of the references to color in this figure legend, the reader is referred to the web version of this book.)

using externally applied electric fields. This has given rise to a number of transmissive and reflective diffraction structures whose diffraction efficiency can be modulated on a gray-scale basis (Bowley, Fontecchio, Lin, Yuan, & Crawford, 1999; Bunning *et al.*, 1995, 1996). The starting syrups are a one-phase homogeneous mixture of LCs mixed with reactive monomer. The anisotropic photopolymerization induced by the interference of coherent beams can result in small, sub 50 nm nanodroplets of LCs which are arranged in a periodic arrangement as shown in Figure 12.

This is in contrast to classic, random two-phase structures shown in Figure 12a which have been studied extensively as dynamic scattering systems (Drzaic, 1995). Matching the field-on refractive index of the phase separated domains with the polymer host results in a transparent film as the field is applied. In the grating case, the local volume fraction of the phase





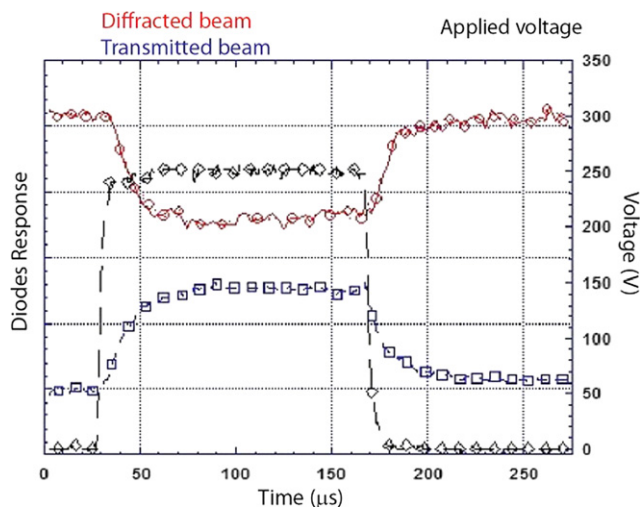
Luciano De Sio et. al

**Figure 13** Cartoon of a transmission grating architecture with the field off (i.e., diffracting) and field on (transmitting) and a representative diffraction efficiency plot as a function of field showing the switch from diffractive to transmitting (a). Cartoon of a reflection grating architecture in the field off and on states (b). The transmission of the film with field off and on is shown in the lower right.

separated LCs can be modulated depending on the writing conditions. Periodic regions of phase separated LC domains exist between periodic regions of pure polymer and the resultant index contrast leads to an optical grating. The difference in local refractive index between the polymer-rich and LC-rich regions enables thin films with very large diffraction efficiency which can be modulated with gray-scale control using an electric field. The nuances of the electro-optic behavior are controlled by the rich variety of two-phase nanostructures that can be formed (Vaia, Tomlin, Schulte, & Bunning, 2001). Typical electro-optic behavior of these films is shown in Figure 13.

Transmission gratings switch from near 100% diffraction efficiency to a null with applied field. Diffraction efficiencies near zero occur when there is an index match of the domains in the switched state to the polymer matrix (similar to classic PDLC systems) (Drzaic, 1995). Considerable polarization dependencies can be observed depending on the morphology of the film and the specific anchoring of the LC within the nanodroplets. Switching times (on and off) on the order of microseconds are typically observed as shown in Figure 14.





Luciano De Sio *et. al*

**Figure 14** Response time for representative sample showing sub millisecond switching for both direction. The pulse shape is shown as a function of time along with the diffractive and transmitted beams responses.

The unusually fast off-times for a nematic LC material are due to the small domain size of the phase separated LC domains. For the reflection grating case, a typical 10  $\mu\text{m}$  thick film exhibits diffraction efficiencies on the order of 70–80% and upon application of a field, the films become optically transparent as shown in Figure 13b. The large index contrast coupled to the fast speeds is a unique attribute not present in other dynamic materials including thermo-optic polymers, electro-optic polymers, or bulk liquid crystals. By controlling the wavelength of exposure and the angle between the two interfering beams during the fabrication, reflection gratings with starting notch reflectivity across the visible and into the NIR region can be formed as shown in Figure 15.

Some blue scatter is always present when observed in transmission, due in large part to both the dispersion of the LC media in this wavelength regime and scatter from the two-phase system. Typical fields needed to switch these films are 5–10 V/ $\mu\text{m}$ , which is the number one drawback of such systems. Improvements to the field strengths can be obtained by introducing specialty monomers and additives into the system, but in general a large surface to volume ratio is introduced by such small size droplets (Schulte, Clarson, Natarajan, Tomlin, & Bunning, 2000). Fluorinated monomers which reduce the surface energy and thus the interaction of the polymer and LC molecules

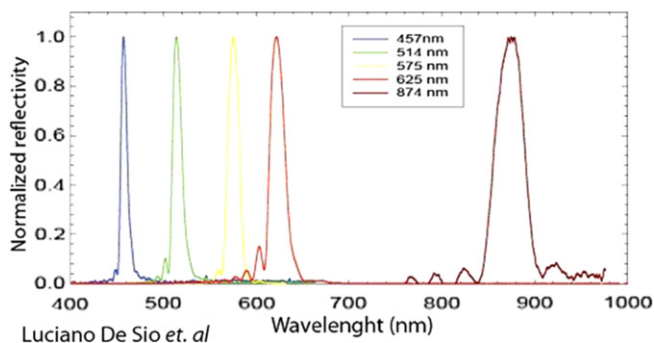


**Figure 15** Spectral shape and position of a variety of reflection grating samples written with appropriate chemistries and geometries to enable reflective properties through the red and into the NIR spectral region. (For interpretation of the references to color in this figure legend, the reader is referred to the web version of this book.)

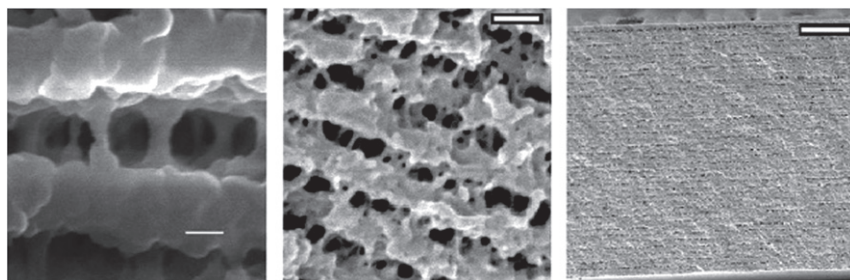
at the boundaries and the addition of inert surfactant molecules (Klosterman et al., 2004; Liu, Sun, Dai, Liu, & Xu, 2005) which act to minimize this surface interaction have been moderately successful in reducing these fields.

Numerous examinations exist on coupling the performance of such systems to the theoretical physics which dictate grating performance (Montemezzani & Zgonik, 1997; Sutherland, 2002). In general, good agreement between theory and experiment exists both in the final optical properties but also in the dynamic evolution of such properties. Variables including the refractive index of both LC and host polymer along with dispersion, droplet size and shape, LC anchoring direction and ordering within the droplets, recording geometry and photoinitiator kinetics have all been examined. Models predicting both the spectral and angular dependence of diffraction efficiency for both transmission and reflection geometries have been successful. Key to the large diffraction efficiency which drives optical performance is the control of the refractive index difference between the polymer-rich and polymer-poor “layers” (Meng et al., 2005). A 50/50 fraction of the two distinct layers and a large local volume fraction of the inert material within its “layer” is generally valued. The ability to obtain such a structure is greatly dependent on the balance between the polymerization, phase separation, and anisotropic diffusion kinetics. If polymerization happens too quickly, then there is not enough time in a low viscosity environment for the non-reacting species to be “transported” toward the null in the interference pattern. A random one- or two-phase morphology will result. If polymerization takes place exceedingly slow, again depending on the compatibility of the non-reactive species with the growing polymer matrix, a random one- or two-phase

morphology will exist. It is only under those conditions where the kinetics of the polymerization and phase separation is appropriately matched with the mass transport kinetics dictated by the size, shape, and periodicity that anisotropic, heterogeneous two-phase morphologies can be formed.

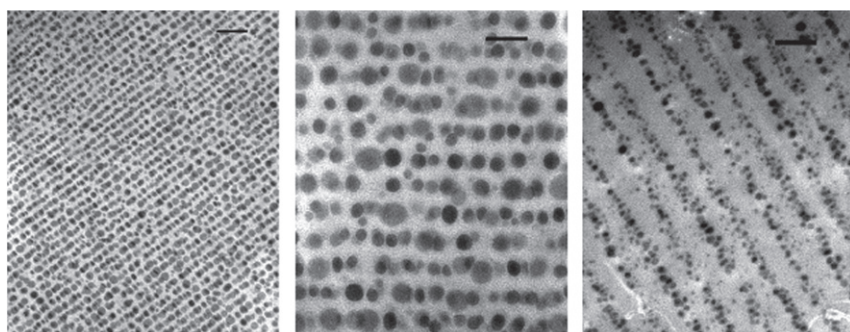
For HPDLC systems, two major classes of monomers have been used which result in morphologies and thus electro-optical properties which are considerably different. For material systems fabricated from acrylate-based monomers using standard UV-writing conditions, well-defined transmission and reflection-based gratings can typically be formed if the period is less than 750 nm. Two different volume fractions of LC domains exist within a periodic, heterogeneous two-phase morphology including a global volume fraction across many periods and the local volume fraction within the LC-rich region itself. Although both are related to the starting position on a phase diagram, the latter is greatly influenced by the complex play of kinetics. Transmission grating structures larger than 750 nm can be fabricated although enabling good confined phase separation of the LC domains becomes increasingly difficult due to a mismatch in kinetics. As the period becomes much larger than several microns, the periodic two-phase structure is typically smeared out and much less confinement of the phase separated domains is observed. The amount of anisotropy of the LC droplets decreases as well as the Bragg spacing is increased. Both the global and the local volume fractions are decreased in this case as more LC is typically trapped in the polymer material (i.e., there is a finite solubility of the LC in the polymer structure). In order to maximize the local volume fraction, a finite balance exists between the starting LC concentration in the syrup, the Bragg spacing, and the kinetics of photopolymerization. For very small Bragg spacings necessary for reflection gratings in the visible, typically the fraction of the grating spacing consisting of the LC-rich regions is between 40% and 50% and highly interconnected domains that are non-spherical are observed (Figure 16).

For HPDLC systems that are formed from thiolene-based photochemistry mixtures, the morphology is fundamentally different (Natarajan et al., 2006; Senyurt, Warren, Whitehead, & Hoyle, 2006). Because the polymerization reaction is step-growth, the system evolves as two immiscible fluid phases until the gelation (solidification) point is reached in the polymer-rich phase. This is in contrast to free-radical systems which form high MW polymer almost immediately inducing almost immediate gelation and thus local phase separation. The major consequence of this type of polymerization is that individual near-spherical domains are typically formed (Figure 17) due to surface tension effects.



Luciano De Sio et. al

**Figure 16** Typical internal morphologies as observed by BF-SEM of reflection gratings written with acrylate chemistry. The scale bar corresponds to 40 nm, 150 nm, and 1500 nm from left to right. The images clearly show the two distinct regions where there are planar continuous but tortuous LC regions separated by crosslinked polymer.



Luciano De Sio et. al

**Figure 17** Typical internal morphologies as observed by TEM of reflection gratings written with thiol-ene chemistry. The scale bar corresponds to 1800 nm, 75 nm, and 650 nm from left to right. The images clearly show individual smooth, spherical-like droplets which are disconnected from each other.

Droplet coalescence can be observed in small spacing systems (reflection gratings) where the initial concentration of LC is high. Thus, morphologies reminiscent of the transmissive-based POLICRYPS structure (discussed in the next section) have been observed in a HPDLC reflection geometry (Abbate et al., 2006; Caputo et al., 2009; De Sio, Serak, et al., 2010). The net consequence of this different morphology is that the switching voltages tend to be much smaller and the scattering lower for systems where gelation takes place much later in the fabrication.

Multi-dimensional, electro-optic structures (photonic crystal structures) fabricated through the use of multiple beam experimental setups have also been enabled in a manner similar to the rich literature on interference holography (Campbell et al., 2000). Complex holographic photopolymerization of monomer/LC mixtures using 2D and 3D writing geometries has lead to a variety of photonic crystals whose electro-optical properties can be modulated. Different lattice types can be readily generated including orthorhombic, face-centered cubic, transverse square, diamond-like, and Penrose structures. Several different exposure geometries and procedures have been employed (Bowley et al., 2000). Photonic crystals written in HPDLC materials show the typical field-dependent diffraction efficiencies and some unusual polarization properties inherent in diffractive structures.

For applications that require a complete bandgap, the index modulation between the polymer and the LC is considerably too low although dynamic modulation (gray-scale) between angle-dependent diffraction and a transparent on-state is enabled. Much larger index modulations (Figure 18) are obtainable by removing the LC but then all dynamic behavior is lost. Changes in the optical structure due to absorption of chemical species can be utilized as a sensitive detection scheme. Complex read-many, write once images can also be fabricated as indicated in Figure 19 (Natarajan, Sutherland, Tondiglia, Bunning, & Adams, 1996). By interfering one of the beams with a second beam which is reflected from a complex surface, a dynamic hologram can be created. Figure 19a shows both faces of a coin, a penny for a size reference, and the thin film in which a hologram of the surface of the coin was written (as indicated, the film is transparent). Figure 19b shows a projection of a laser through the film and expanded which

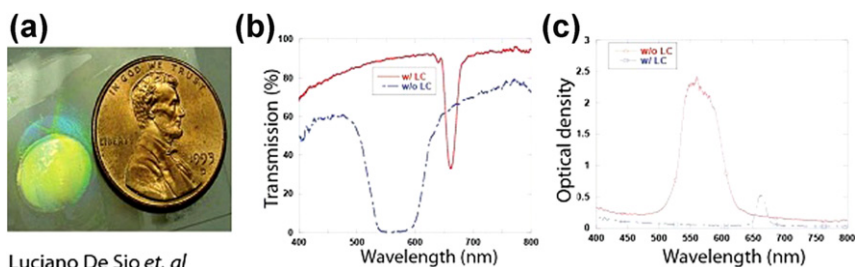
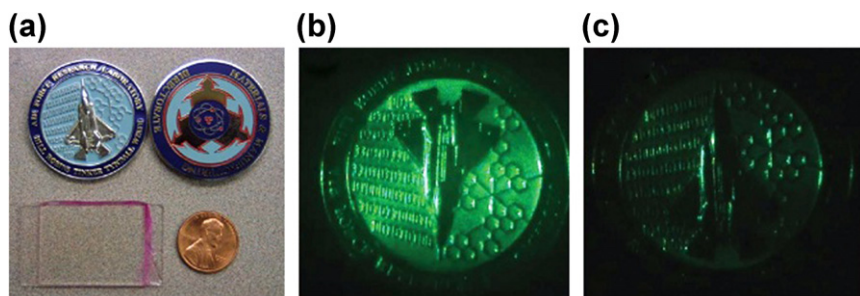


**Figure 18** Image of reflection grating written in 10  $\mu\text{m}$  thick HPDLC syrup after removing the LC as related to the size of a penny (a). The transmission (b) and reflection (c) properties of the as-written and LC-removed gratings are shown. The notch depth increases substantially as does the bandwidth of the reflection peak due to much increased refractive index contrast.



Luciano De Sio et. al

**Figure 19** (a) Complex hologram formed from the interference of a reference beam with that reflected from the shiny surface of a coin. The hologram as formed is transparent; (b) is the projected image from the thin film showing the fine detail captured during the writing process. (c) Shows greatly reduced contrast upon application of a voltage.

clearly shows the detail originally observed on the surface of the coin. Figure 19c shows a “black” screen after applying a field across the cell. The image contrast is erased upon application of a field due to the reorientation of the LC molecules within the domains, providing an index match which erases the information written in the initial exposure. Turning the field off returns the hologram to the read condition. Any reflective surface can be used to write the image. The largest variation of work on varying the structure and thus property of such systems has been on varying the exposure conditions. Parameters including intensity, length of exposure, and wavelength have been extensively studied. This last variable opens up a variety of photochemistries through the use of wavelength specific photo-initiators. A subtle balance exists between the polymerizations kinetics, the phase separation process, and the underlying diffusion processes which occur during exposure. From a material perspective, a variety of different monomers have been employed where one is balancing the initial homogeneity and compatibility of the reactive syrup to the final structure. Variations have centered on modifying the initial functionality of the system which affects both the polymerization and phase separation kinetics and on incorporating fluorine-based monomers to affect the anchoring (Pogue et al., 2000). Each change in monomer type necessitates a new optimization with respect to optimum LC concentration in the starting mixture and the most appropriate exposure conditions. Large changes in properties are obtained from utilizing step-growth monomers (typically thiolenes) which are exposed using visible photochemistry instead of the typical free-radical, UV-induced photopolymerization. Structures which much more homogeneous internal



morphologies are obtained which decreases the scattering due to heterogeneity in any two-phase composite and typically reduces the switching voltages. Being able to cure out in the visible is a necessity for the fabrication of reflection gratings with optical notch's residing past 600 nm. Continued developments in materials and processes to enable HP in the red and longer wavelengths continue to be one of the major challenges for reflection gratings.

The formation of such structures using holography, liquid crystals, and photochemistry also enable a wide variety of related constructs. Introduction of azo-LC media allows the formation of photosensitive grating structures (De Sio, Serak, et al., 2010; Urbas, Beckel, Tondiglia, Natarajan, & Bunning, 2006). Instead of modulating the diffraction properties using an electric field, light of a suitable wavelength can be utilized to introduce isothermal phase changes (and thus refractive index changes). Molecules such as azo-based dopants and LCs can be introduced. Irradiation with the proper wavelength will lead to substantial changes in molecular order within the LC nanodroplets due to trans-cis isomerization processes. This modulation of the local refractive index due to these changes leads to dynamic photonic behavior which is controlled by both the wavelength and intensity of incoming light.

The marriage between HP and LCs has brought ample research opportunities for the development of dynamic photonic structures. Future research should focus on fabricating multi-functional, multi-responsive structures, and achieving better property control by fine-tuning the competition between phase separation and photopolymerization processes. This can be achieved by better control of the laser curing process, local control of temperature, better starting compatibility between the reactive and non-reactive components of the starting syrups, and designer monomer mixtures. Studying dynamic changes to these periodic, nanoscale structures induced by electrical, thermal, optical, or magnetic stimuli using high resolution spectroscopy, X-ray/neutron scattering, and high resolution microscopy techniques will provide many future opportunities.



## **4. POLICRYPS STRUCTURES**

### **4.1 Realization and Theoretical Model**

In general, both transmission and reflection HPDLC gratings exhibit good optical and electro-optical (switching) characteristics, and reliable overall performances. In some cases, however, these can be affected by some scattering

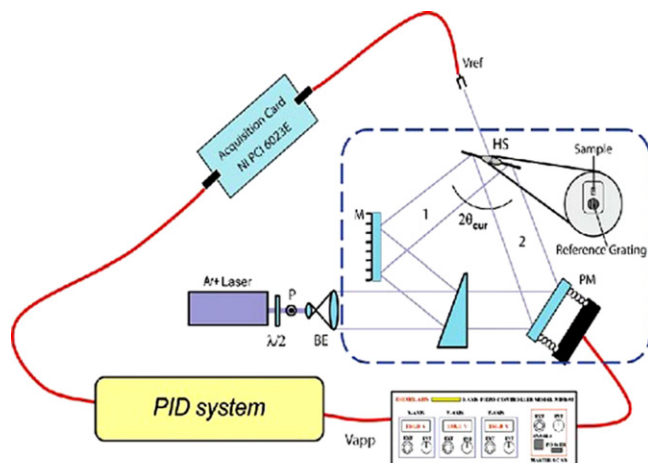
of the impinging light, if its wavelength is comparable with the average size of the LC droplets; thus, a new type of switchable, transmission grating has been recently realized and studied (Caputo, De Sio, Sukhov, Veltri, & Umeton, 2004; Caputo, Sukhov, Umeton, & Veltri, 2005). It is called “POLICRYPS,” acronym of “PO-lymer LI-liquid CRY-stal P-olymer S-lices, and is made of slices of almost pure polymer alternated to films of almost pure NLC, whose director is uniformly aligned perpendicularly to the polymeric slices. In this new kind of switchable diffraction grating, the absence of NLC droplets prevents light scattering and allows fabrication of structures with a high optical quality, independently of the particular value of the impinging wavelength; indeed, in some samples, a diffraction efficiency as high as 98% has been measured. Furthermore, confinement and alignment of NLC molecules in uniform films enable an electric field of few V/ $\mu\text{m}$  to reorient the NLC director in a millisecond timescale; similarly to the HPDLCs case, by suitably choosing the polymer refractive index and the ordinary/extraordinary refractive indices of the NLC, this reorientation can be exploited to switch on/off the spatial modulation of the structure average refractive index, experienced by an impinging light beam, thus switching on/off the grating diffraction efficiency.

#### 4.1.1 Fabrication Recipes

The standard POLICRYPS fabrication procedure exploits the interference pattern of a UV radiation ( $\lambda = 0.351 \mu\text{m}$ ), impinging on a mixture of NLC (at high temperature, in the isotropic phase), photo-initiator and monomer molecules. A high diffusivity, due to the high temperature, of the mixture components prevents the local nucleation of NLC droplets and brings out a spatially periodic polymerization of the monomer, thus forming the “polymeric slices,” while all NLC molecules are confined in pure NLC films between the slices. The sample is, then, cooled down below the Isotropic–Nematic transition point, with a slow rate. The experimental setup (Figure 20) exploits an active stabilization system for the suppression of vibrations and allows to set the spatial period of the grating in the range  $\Lambda = 0.2\text{--}15 \mu\text{m}$ , by adjusting the curing interference angle (De Sio, Caputo, De Luca, Veltri, & Umeton, 2006).

The exposed procedure has been recently implemented in a further “multi-step” procedure, which allows substituting the NLC between the polymeric slices with different soft materials (De Sio, Ferjani, Strangi, Umeton, & Bartolino, 2011). In fact, while keeping the POLICRYPS above the Nematic–Isotropic transition temperature, an etching process washes out the





Luciano De Sio et. al

**Figure 20** Optical holographic setup for UV curing gratings with stability check: P, polarizer;  $\lambda/2$ , half-wave plate; BE, beam expander; BS, beam splitter;  $2\theta_{\text{cur}}$ , total curing angle; M, mirrors; S, sample; PD<sub>1</sub>, first beam photodetector; PD<sub>2</sub>, second beam photodetector; PD<sub>3</sub>, diffracted and reflected beam photodetector. Inset: Reference grating (positioned immediately below the sample area) that enables the stability check. *Reproduced from De Sio et al. (2006).*

NLC and any eventual unpolymerized component from the structure. In this way, a template is obtained, which is made of sharp polymer slices separated by empty channels; these one, in a final step, can be filled, by capillary flow, with any desired material.

#### 4.1.2 Theoretical Model for Composite Structures Formation

Taking into account both molecular diffusion and chemical reactions that occur during the UV-induced formation (the “curing”) of the composite structure (Veltri, Caputo, Umeton, & Sukhov, 2004), it has been implemented a theoretical model that satisfactory explains how/when both HPDLC or POLICRYPS morphologies can be obtained. It shows indeed that two control parameters, related to the diffusivity of the different mixture molecules ( $B$ ) and to the intensity of the curing UV radiation ( $G$ ), govern the whole process: Both HPDLC or POLICRYPS kind of samples can be obtained by simply choosing suitable values of  $B$  and  $G$ . In particular, it has been shown that both low curing intensity and low temperature values are requested in order to obtain HPDLC grating, while realization of a POLICRYPS grating needs that a higher diffusion of monomer molecules takes place during the

curing process; this means that the “curing temperature” has to be set above the Nematic–Isotropic transition. The model considers a sample of length  $L$  in  $z$  and infinite in  $x$ - and  $y$ -directions, filled with a mixture of NLC, monomer, and photo-initiator (in concentrations  $C$ ,  $M$ , and  $I$ , respectively); the sample is cured by a UV interference pattern  $W(x)$ , whose wavevector  $q$  is directed along the  $x$ -axis. By exploiting a classical reaction scheme for the radical polymerization (Atkins, 1987), assuming that all mass transfer processes are driven by Fick diffusion and under reasonable assumptions and approximations (details in Veltri et al., 2004), the whole formation process of the composite structure is governed by the following three coupled equations:

$$\begin{cases} \frac{\partial \mu}{\partial \tau} - B \frac{\partial}{\partial \xi} \left[ (1 - \nu)^{\frac{2}{3}} \frac{\partial}{\partial \xi} \frac{\mu}{1 - \nu} \right] + (1 + m \sin \xi)^{1/2} \mu = 0, \\ \frac{\partial \nu}{\partial \tau} = \frac{G(1 + m \sin \xi)}{2} \left[ N_0^2(1 - \gamma) + N_0(1 + \gamma) + \frac{2\gamma}{1 - \gamma} \right] \gamma^{N_0}, \\ \frac{\partial \sigma}{\partial \tau} - B \frac{\partial}{\partial \xi} \left[ (1 - \nu)^{\frac{2}{3}} \frac{\partial}{\partial \xi} \frac{\sigma}{1 - \nu} \right] = 0, \end{cases} \quad (1.4)$$

where

$$B = \frac{4\pi D(k_t)^{1/2}}{(gW_0I)^{1/2}\Lambda^2}; \quad G = \frac{(k_t g W_0 I)^{1/2}}{k_p T}; \quad \gamma = \frac{1}{1 + \frac{G\sqrt{(1+m\sin\xi)}}{\mu}}. \quad (1.5)$$

The system is written in a reduced form:  $\sigma = C/T$ ,  $\mu = M/T$ , and  $\nu = P/T$  are the relative concentrations of components ( $P$  stands for the polymer concentration and  $T$  for the total molecular concentration), while  $\tau = \{(k_p/k_t)[k_t g W(x)I]^{1/2}\}t$  is a dimensionless time;  $k_p$  and  $k_t$  are the chemical prolongation and termination constants for the polymer formation reactions (Atkins, 1987), and  $t$  is the time;  $g$  represents the activation probability of the initiator molecules when acted on by the UV curing radiation. In addition,  $D$  is the monomer diffusion constant and  $N_0$  is the least number of monomer molecules needed to form of an immobile polymer chain. The local intensity of the curing pattern is  $W(x) = W_0[1 + m \sin(\xi)]$ , where  $W_0 = (I_1 + I_2)$  is the total intensity ( $I_1$  and  $I_2$ , intensities of individual beams) and  $m = 2[I_1 I_2]^{1/2}/(I_1 + I_2)$  is the fringe contrast;  $q = 2\pi/\Lambda$ , where  $\Lambda$  is the fringe spacing and  $\xi = qx$ . In the framework of a numerical approach to the solution of the above equation system (an analytical solution has been derived only for some, particularly simple, case (Veltri et al., 2004)), spatial derivatives have been performed by utilizing a central derivative scheme, while temporal

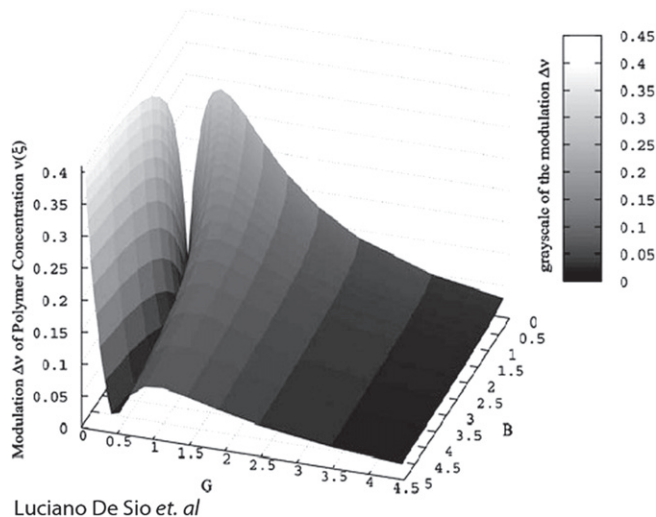


**Figure 21** Modulation of the polymeric concentration  $\Delta v(\xi)$  as a function of parameters  $B$  and  $G$  on a three-dimensional surface. *Reproduced from Veltri et al. (2004).*

derivatives have been calculated by exploiting a second order Runge–Kutta scheme. Finally, the modulation  $\Delta v(\xi)$  of the polymeric concentration  $v(\xi)$  has been calculated as its first spatial Fourier component.

The function  $\Delta v(\xi)$ , which is directly related to the diffraction efficiency of the grating, is plotted in Figure 21 as a function of  $B$  and  $G$  (in the case  $N_0 = 4$ ). Two regions of high grating diffraction efficiency (high  $\Delta v(\xi)$  values) can be clearly singled out:

- $B \ll 1$ . Polymer chains rapidly grow before monomer diffusion takes place; thus, gratings formed under this condition are made of slides rich in LCs and short polymer chains, alternated with other slices made of long, immobile, polymer chains. HPDLC gratings have been realized in experimental conditions coherent with the values that parameters  $B$  and  $G$  assume in this region (Caputo et al., 2004).
- $G \ll 1$  with  $B > 1$ . The polymerization reaction is quite slow and monomers can diffuse across the fringes before reacting with any other molecule. Thus, because there is a high number of available radicals only in the bright fringes (low curing intensity), it is more probable for a chain to be closed by a radical than to get a new monomer; polymerization takes place mainly in these fringes. POLICRYPS gratings have been fabricated in the corresponding experimental conditions.

## 4.2 Applications of NLC-Based POLICRYPS

### 4.2.1 Switchable Holographic Grating

The first POLICRYPS-based device was an electrically switchable transmission grating, a structure that, in principle, can completely diffract or transmit an impinging light beam, following the application of an external electric field. Results related to an experimental comparison between a standard HPDLC and a POLICRYPS grating, both of them fabricated with the same fringe spacing, cells thickness, and initial mixture ( $\Lambda = 1.5 \mu\text{m}$ ,  $L = 16 \mu\text{m}$ , 30% in weight of 5CB NLC in NOA61 pre-polymer), put into evidence the better overall performances of the second sample (Caputo et al., 2004). A weak He-Ne probe laser beam ( $\lambda = 633 \text{ nm}$ ) is used to measure, for both structures, the first order diffraction efficiency ( $\eta_1 = T_1/T_{\text{tot}}$ , where  $T_0$ ,  $T_1$ , and  $T_{\text{tot}} = T_0 + T_1$  indicate the zeroth order, the first order, and the total transmittivity, respectively). Measured values turn out to be:  $\eta_{1(\text{HPDLC})} \approx 44\%$  and  $\eta_{1(\text{POLICRYPS})} \approx 93\%$ .

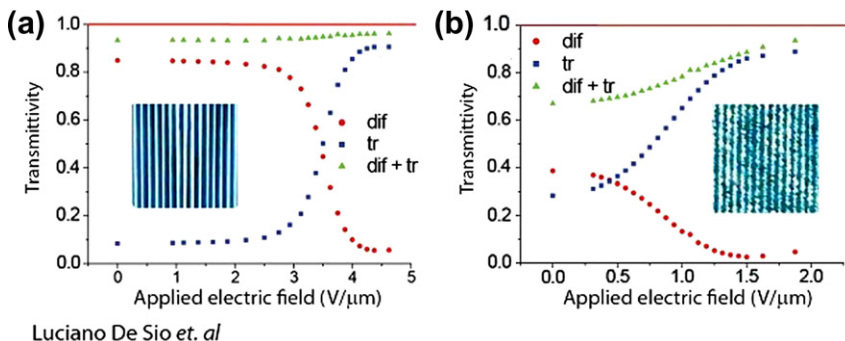
An electro-optical characterization has been performed by using the ITO covered glass slabs of samples to apply them a low frequency electric field. For the POLICRYPS, Figure 22a shows the dependence of  $T_1$ ,  $T_0$ , and  $T_{\text{tot}}$  on the external electric field: As the field increases, the on/off switching of  $T_1$  and the simultaneous off/on switching of  $T_0$  appear quite sharp; it is also evident that  $T_{\text{tot}}$  always remains at almost the same high value, thus demonstrating that scattering losses are negligible. The situation is quite different for the HPDLC grating (Figure 22b): in this case, not only observed switches of both  $T_1$  and  $T_0$  are quite smooth, but  $T_{\text{tot}}$  remains well below 1 and increases as the applied field increases.

Further experimental investigations (Caputo et al., 2005) have shown that the dependence of  $\eta_{1(\text{POLICRYPS})}$  on some typical geometrical and physical parameters can be interpreted in the framework of the Kogelnik model (Kogelnik, 1969) according to the expression:

$$\eta = \sin^2 \left( \frac{\pi(\varepsilon_1 \varepsilon_{-1})^{1/2} L}{\sqrt{\varepsilon_0} \lambda \cos \beta} \right) = \sin^2(\Psi(L, \lambda, T)), \quad (1.6)$$

where  $\lambda$  is the wavelength of the probe radiation in vacuum,  $L$  the cell thickness,  $\varepsilon_i$  ( $i = 1, -1$ ) stands for the  $i$ th Fourier component of the dielectric function across the fringe,  $\beta$  is the refraction angle of the probe beam inside the sample,  $T$  the temperature.

Application of an external electric field to the POLICRYPS is not the only means to realize a switching of its refraction efficiency. By adding a small concentration of azo LCs (Hrozyk et al., 2006) in the initial mixture, and



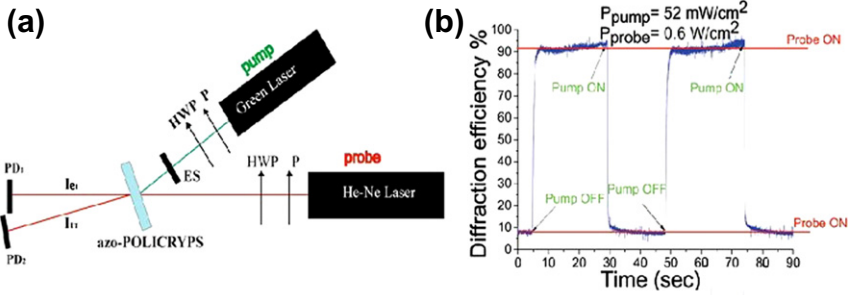
Luciano De Sio et. al

**Figure 22** Dependence on an applied electric field of  $T_0$  (squares),  $T_1$  (circles) and  $T_{tot}$  (triangles) for: (a) POLICRYPS grating and (b) HPDLC grating, at room temperature. Pictures in the insets show a typical POLICRYPS and HPDLC grating morphology, respectively, observed with a Polarizing Optical Microscope. Reproduced from [Caputo et al. \(2004\)](#).

exploiting the “multi-step” fabrication process ([De Sio, Ferjani, et al., 2011](#)), high quality POLICRYPS gratings have been realized, which can be optically controlled in the visible range ([De Sio, Serak, et al., 2010](#)). The sample operation has been investigated by means of the setup of Figure 23a: a green diode laser ( $\lambda = 532$  nm) represents the pump source, while the probe beam,  $p$ -polarized to experience the highest diffractive index modulation in the sample ([De Sio, Serak, et al., 2010](#)), comes from a He–Ne laser ( $\lambda = 633$  nm). Figure 23b reports  $\eta$  variations induced by the pump green light. When switched on, it produces a trans–cis photoisomerization of the azo-LC molecules ([Hrozhyk et al., 2006](#)), which strongly affects the NLC director orientation; only an average NLC refractive index, very close to the value of the polymeric one, is experienced by the probing beam, with a consequent drop in the value of  $\eta$ . When the pump beam is switched off, a reverse cis–trans photoisomerization of azo-LC molecules takes place, which induces a reorientation of the NLC director, thus restoring a high spatial modulation of the sample diffractive index, experienced by the  $p$ -polarized probe light, and thus a high  $\eta$  value. Figure 23b shows also that the azo-POLICRYPS exhibits both fast spontaneous relaxation and fast photoisomerization responses.

#### 4.2.2 Switchable Beam-Splitter

An Optical Beam Splitter (OBS) has been realized, which exploits an azo-POLICRYPS working in the “Bragg grating” regime (only the first diffraction order is observed in addition to transmission ([De Sio, Tedesco, Tabiryan, &](#)



Luciano De Sio et. al

**Figure 23** Experimental setup for the observation of all-optical operation of POLICRYPS diffraction gratings containing azo-LC (a). PD<sub>1,2</sub>: photodetectors; HWP: half-wave plate; P: polarizer; ES: electronic shutter. Changes of the diffraction grating efficiency induced by a pump green light (b). Power density values are indicated in the figure. *Reproduced from De Sio, Serak, et al. (2010).*

Umeton, 2010)). The used experimental setup is shown in Figure 24, along with a Mach–Zehnder interferometer; here, combination of the transmitted and first diffracted beams produces an interference pattern, whose fringe visibility  $V$  is optically controlled. The experimental geometry is adjusted to ensure a maximum  $\eta$  value  $\eta_{\max} \approx 50\%$ , when the pump beam is off (Bücher et al., 1974). The detector PD is used to measure both the maximum ( $I_{\max}$ ) and minimum ( $I_{\min}$ ) intensity values along the interference pattern; it is possible, therefore, to evaluate  $V$ , defined as  $V = (I_{\max} - I_{\min}) / (I_{\max} + I_{\min})$ . On the other hand,  $V$  depends on the ratio  $R = I_{1T} / I_{0T}$  of the intensities of the first diffracted and transmitted beams:  $V = [2(R)^{1/2} / (1 + R)]$  (De Sio, Tedesco, et al., 2010); thus, being  $R = \eta / (1 - \eta)$ ,  $V$  depends on  $\eta$  according to  $V = 2[\eta(1 - \eta)]^{1/2}$ . In the azo-POLICRYPS grating,  $\eta$  varies with the power  $P_{\text{pump}}$  of the impinging pump beam; therefore, the device operation can be studied by plotting  $V$  versus  $P_{\text{pump}}$ . Measured values of  $R$  and  $V$  are reported in Figure 25 versus  $P_{\text{pump}}$ .  $R$  values can be finely adjusted between 1 (when the pump light is off ( $\eta = \eta_{\max} \approx 50\%$ ), and 0 (only transmitted, no diffracted beam). Measured  $V$  values are switched from 0.94 to 0.2, in good agreement with calculated ones (1 and 0, respectively). Devices of this kind can be exploited to investigate those materials in which a tunability of the impinging light intensity profile is necessary to study their non-linear properties.

#### 4.2.3 Switchable Waveplate

Birefringent materials can be used for the fabrication of retardation plates: Light with wavelength  $\lambda$ , propagating through a birefringent sample,

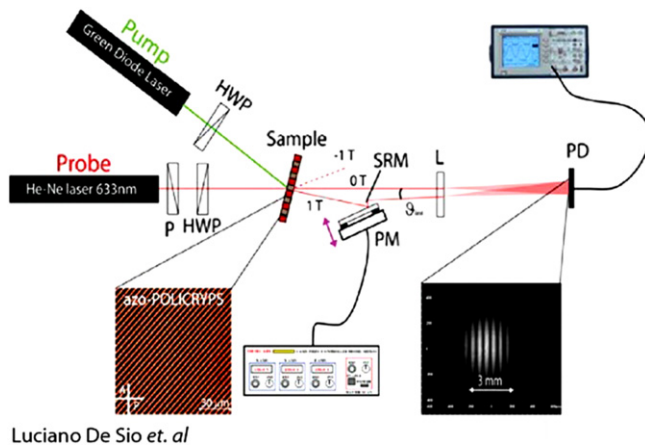


**Figure 24** All-optical OBS and interferometer setup: P, polarizer; HWP, half-wave plate; SRM, semireflective mirror;  $\vartheta_m$ , interference angle; PM, piezomirror; PD, photodetector; L, lens. Reproduced from *De Sio, Tedesco, et al. (2010)*.

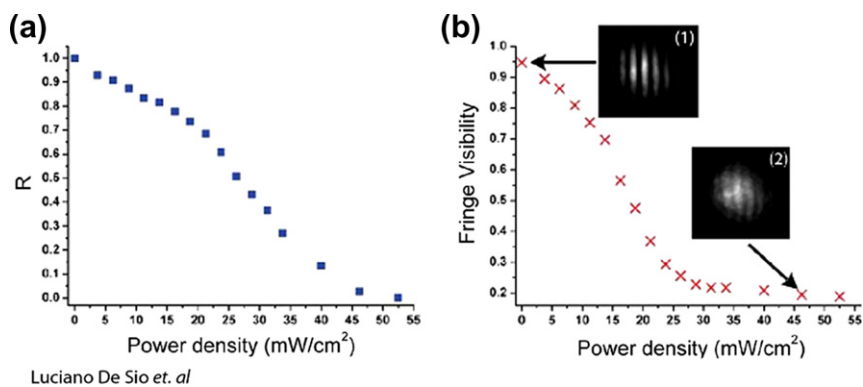


**Figure 25** Beam splitting (a) and fringe visibility (b) versus the pump power density. Interference patterns acquired with a CCD camera are drawn for  $V = 0.94$  (inset 1) and  $V = 0.2$  (inset 2). Reproduced from *De Sio, Tedesco, et al. (2010)*.

separates into an ordinary and an extraordinary component that travel with different velocities. At the exit of the sample, the two waves recombine with a phase difference  $\delta$ , which depends on the value  $\Delta n$  of the cell birefringence according to the expression  $\delta = 2\pi L \Delta n / \lambda$ , where  $L$  is the sample thickness. A planarly aligned NLC cell, acted on by an electric field  $E$  applied perpendicularly to the cell plates, represents a tunable retardation plate: Under the action of  $E$ , the molecular director reorients along it, with a consequent variation in  $\Delta n$  and thus in the phase difference  $\delta$  between the two



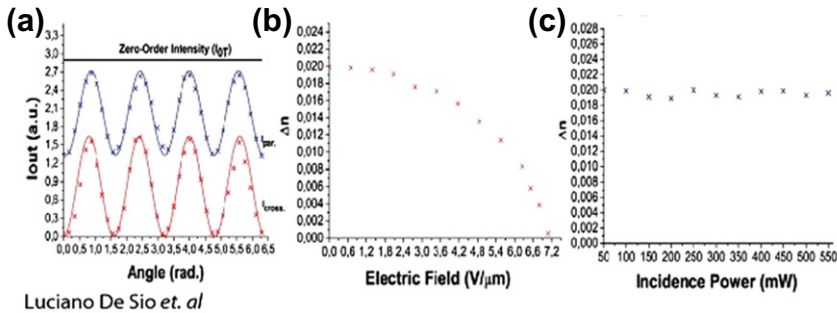


**Figure 26** Output intensity versus the rotation angle  $\alpha$  obtained by placing the sample between crossed (red) and parallel (blue) polarizers (a). Birefringence versus the applied electric field (square voltage pulses at 1 kHz) (b). Birefringence versus the power of the impinging laser beam (c). (For interpretation of the references to color in this figure legend, the reader is referred to the web version of this book.) *Reproduced from De Sio et al. (2008).*

components which an impinging light wave is decomposed into; since the director reorientation angle depends on  $E^2$ , variations in this value yield a tuning of  $\delta$ . However, a strong sensitivity to temperature variations and quite long switching times may represent a limit of this kind device, and an alternative has been suggested in a suitably fabricated POLICRYPS structure (De Sio, Tabiryan, Caputo, Veltri, & Umeton, 2008). In fact, its polymeric slices exert an action of stabilization of the NLC molecules, thus increasing the sample thermal stability; in addition, quite low voltages are needed to operate the device. In the experimental setup, the light from a He–Ne laser ( $\lambda = 633$  nm) passes through a polarizer before reaching the POLICRYPS, whose optical axis orientation around the propagation direction can be set to any desired angle ( $\alpha$ ). Then, the transmitted light passes through a second polarizer (the analyzer) before reaching the detector (De Sio et al., 2008).

The intensity after the analyzer, measured versus  $\alpha$ , both between crossed ( $I_{\text{cross}}$ ) and parallel ( $I_{\text{parallel}}$ ) polarizers, is shown in Figure 26a: both  $I_{\text{cross}}$  and  $I_{\text{parallel}}$  are periodic functions of  $\alpha$ , which is typical of a retardation plate. When  $\alpha$  is set at  $45^\circ$  with respect to the axes of the two polarizers (parallel to each other), a variation in  $\Delta n$  is obtained by applying an electric field, which is increased from  $E_{\text{in}} = 0$  to  $E_f = 7.1$  V/ $\mu\text{m}$  (this value switches off  $\Delta n$ , Figure 26b). Figure 26c confirms the stabilization action of the POLICRYPS: only small  $\Delta n$  variations are observed when strongly increasing the impinging light intensity. The behavior of a POLICRYPS phase modulator can be interpreted in the framework of the Jones Matrix



formalism (Caputo, Trebisacce, De Sio, & Umeton, 2010). The intensity  $I_{\text{out}}$  of the transmitted light is calculated as:

$$I_{\text{out}}(\beta) = \frac{I_{\text{inc}}}{2} [H^2 \sin^2 \beta + V^2 \cos^2 \beta + HV \sin 2\beta \cos \delta], \quad (1.7)$$

where  $I_{\text{inc}}$  is the impinging light intensity and  $\beta$  is the angle between analyzer and polarizer axes. By setting  $\beta$  at a particular value ( $\beta = \pi/4$ ),  $\delta$  can be experimentally evaluated from the equation (Caputo et al., 2010):

$$\cos \delta = \frac{1}{HV} \left[ \frac{2I_{\text{out}}(\beta = \pi/4)}{I_{\text{inc}}} - \frac{H^2 + V^2}{2} \right]. \quad (1.8)$$

Similarly, parameters  $H$  and  $V$ , which depend on the birefringent material, can be evaluated as:

$$H = \sqrt{\frac{2I_{\text{out}}(\beta = \pi/2)}{I_{\text{inc}}}}; \quad V = \sqrt{\frac{2I_{\text{out}}(\beta = 0)}{I_{\text{inc}}}}. \quad (1.9)$$

#### 4.2.4 Tunable Bragg Filter

POLICRYPS structures have been utilized for the realization of tunable optical filters (d'Alessandro et al., 2008). A high index contrast ( $\Delta n \cong 0.04$ ) channel, in-diffused, waveguide in BK7 glass substrate enables mono-modal propagation of electromagnetic radiation in the optical C-band (1530–1560 nm), with very low propagation losses ( $<1$  dB/cm). On top of the waveguide, a glass slab, spaced by few micron spacers, creates a gap, which is infiltrated with a standard mixture of E7 NLC, NOA61 pre-polymer and curing agent. After UV curing, a POLICRYPS grating, with a spatial periodicity  $\Lambda \approx 2.55$   $\mu\text{m}$ , is obtained (Figure 27). The evanescent wave of a TE-like radiation ( $\lambda \approx 1550$  nm) propagating in the waveguide experiences in the overlaying POLICRYPS a phase grating, due to the mismatch between the E7 ordinary refractive index ( $n_{\perp} \approx 1.5$ , for light polarization perpendicular to the LC director) and the NOA61 one ( $n_p = 1.5419$  at  $\lambda = 1550$  nm). This grating enables the device to operate as a Bragg filter, with a back-reflected (Bragg) wavelength given by  $\lambda_B = (2\Lambda n_{\text{eff}})/m$ , where  $m$  is the diffraction order, and  $n_{\text{eff}}$  indicates the effective refractive index of the guided mode; for  $m = 5$ ,  $\lambda_B$  is in the telecom range. Figure 28a shows the filter transmission spectrum (with a 20 dB suppressed signal at the Bragg wavelength of 1552 nm), obtained when injecting in the guide the radiation from a broadband source, with  $\lambda$  ranging from 1530 nm to 1565 nm (d'Alessandro et al., 2008).

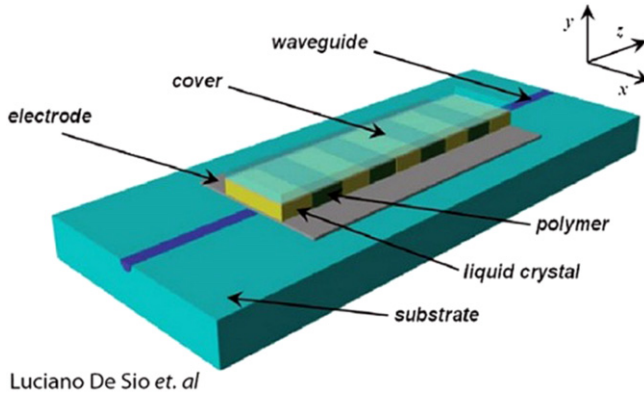


**Figure 27** Sketch of an integrated optical filter including a POLICRYPS grating.

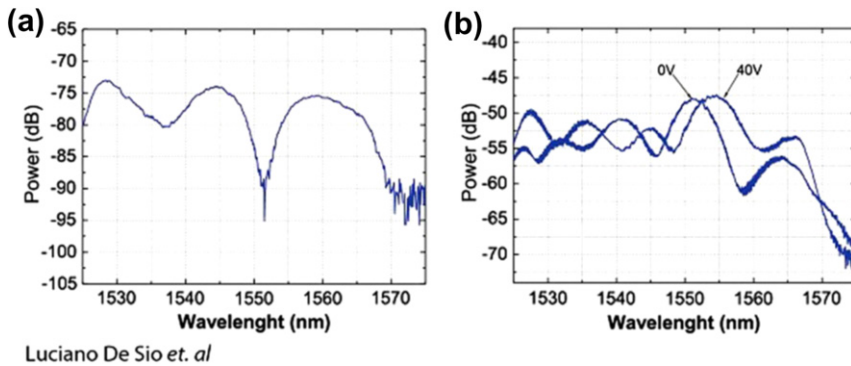


**Figure 28** Transmitted (a) and tuned reflected (b) spectra of the POLICRYPS filter detected by using an optical spectrum analyzer. *Reproduced from d'Alessandro et al. (2008).*

Application of an electric field by means of coplanar aluminum electrodes, patterned on both sides of the channel waveguide, induces an in-plane reorientation of the NLC director inside the POLICRYPS, with a consequent variation in the refractive index modulation of the (overlying) hybrid cladding experienced by the guided radiation, and a tuning of  $\lambda_B$ . An optical circulator, introduced in the same set-up, allows detecting the filter reflected spectrum as well. Figure 28b shows both the reflected spectrum detected with no applied electric field, and the one detected when a square-wave electric field ( $\approx 2.7 \text{ V}/\mu\text{m}$  at 1 kHz) is applied to the device.

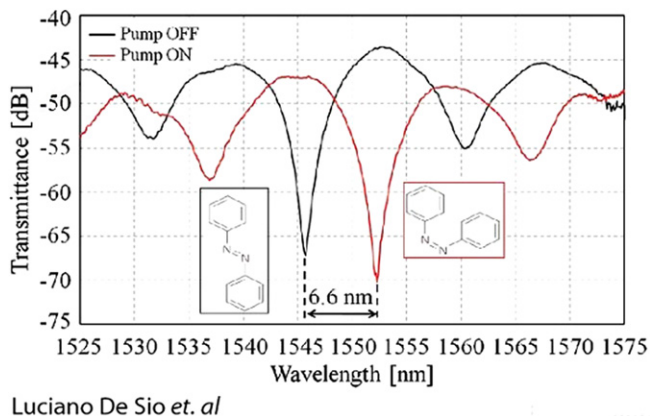


**Figure 29** Transmittance of the all-optical filter. Black line—Pump off; inset: azo dye in trans-phase. Red line—Pump on; inset: azo dye in cis-form. (For interpretation of the references to color in this figure legend, the reader is referred to the web version of this book.) Reproduced from [Gilardi et al. \(2011\)](#).

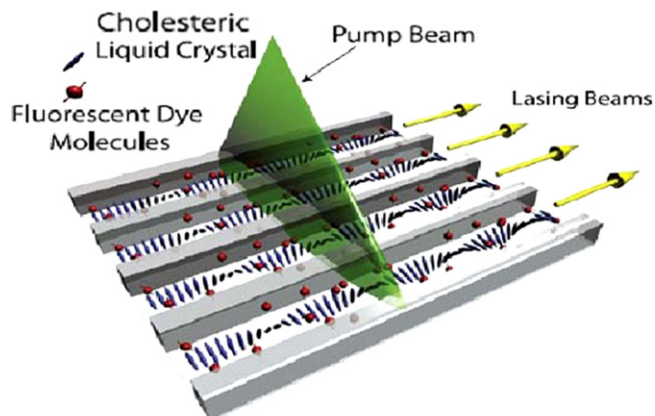
The filter exhibits a Full Width at Half Maximum (FWHM) of about 5 nm, with a tuning range of 4 nm, which can be span by varying the amplitude of the applied electric field. An implementation of the above system is represented by an integrated tunable filter, which enables a full optical tuning of  $\lambda_B$ , realized with an azo-POLICRYPS ([Gilardi et al., 2011](#)). The grating ( $\Lambda \approx 1.5 \mu\text{m}$ ) is fabricated according to the multi-step process ([De Sio, Ferjani, et al., 2011](#)) and exploits the E7 NLC doped with Methyl Red (MR) dye. If no pump light is impinging on the sample, MR molecules are in their elongated (trans) form: both their long axes and the NLC director are aligned perpendicularly to the polymer slices and the sample is optically anisotropic, exhibiting a mismatch (for the TE-like mode) between the refractive index of the NOA61 polymer and the one of the trans-MR + E7 mixture. The device operates as a Bragg filter, with  $\lambda_B$  falling in the telecom range for  $m = 3$ . The black line of Figure 29 shows the transmitted spectrum in these experimental conditions: a notch peak of  $-20$  dB at  $\lambda_B = 1545.7$  nm, with a bandwidth of about 3.3 nm (at  $-3$  dB with respect to the minimum), can be recognized. Irradiation with light at  $\lambda = 532$  nm induces a trans-cis transition in MR molecules, which affects the NLC director orientation; the NLC + MR mixture becomes optically isotropic, with a consequent variation in the mismatch of the refractive indices and a variation in  $\lambda_B$  value; the spectrum is shifted by 6.6 nm, with a notch of  $-22$  dB and a 2.7 nm bandwidth (red line, Figure 29).

### 4.3 Applications POLICRYPS Based on CLC and FLC

#### 4.3.1 Microlaser Array

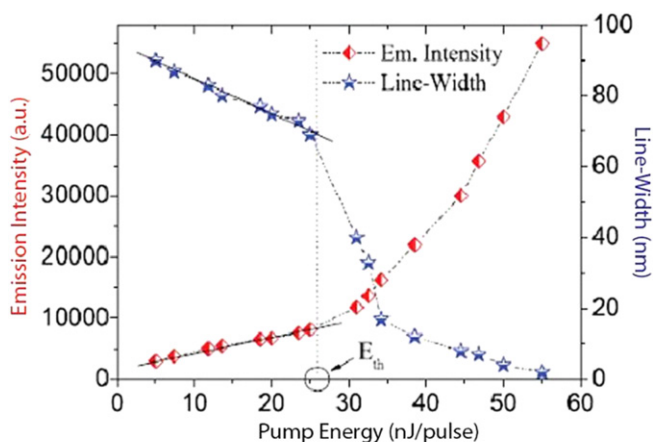
Due to a mechanism known as “distributed feedback (DFB),” a CLC system, under suitable geometrical conditions, behaves as a mirrorless optical resonator, exhibiting a photonic bandgap. If the CLC is doped with dye molecules and acted on by a pump laser, a gain enhancement of the dye fluorescence radiation, propagating in the structure, can be observed (Kogelnik & Shank, 1971). In this framework, a POLICRYPS structure containing dye doped CLC can operate as an array of microlasers (Strangi et al., 2005). Since the POLICRYPS channel lengths are not limited, in general, by the sample geometry and can reach several centimeters (thus including many periods of the CLC helices), while the channel volume can be reduced by reducing the structure pitch, optical resonators (microcavities) with a high quality factor  $Q$  can be fabricated. Indeed, a POLICRYPS laser array has been realized (Strangi et al., 2005), which utilizes a small amount of pyrromethene dye, diluted in BL088 CLC, confined in a NOA61 polymeric structure (pitch  $\Lambda \approx 5 \mu\text{m}$ , microcavity width  $\approx 1.5 \mu\text{m}$ ). The system is pumped with the second harmonic ( $\lambda = 532 \text{ nm}$ ) of a Nd:YAG pulsed laser, focused onto the sample perpendicularly to the orientation of the polymeric channels, to ensure the simultaneous excitation of several microchannels (Figure 30), and linearly polarized perpendicularly to them. A stimulated emission emerges from the microcavities along them, which is circularly polarized, thus demonstrating that a DFB mechanism, due to the CLC helices, drives the observed phenomenon.

At low pump energy, both emission intensity and spectral FWHM show an almost linear dependence on it (Figure 31). Above a typical threshold energy  $E_{\text{th}} \approx 25 \text{ nJ/pulse}$ , the emitted intensity starts to rapidly increase, while the FWHM significantly decreases. Interestingly, the  $E_{\text{th}}$  value is one order of magnitude lower than other systems, under similar physical conditions. The lasing intensity can be controlled by applying an electric field, perpendicular to the helical axis orientation. By maintaining the pump energy at a fixed value, a sinusoidal voltage, applied through the ITO-coated glass slabs that confine the POLICRYPS cell, is varied from 0 up to  $3.7 \text{ V}/\mu\text{m}$  (1 kHz), producing a decrease of the lasing intensity. The effect is explained by taking into account that the applied electric field induces a distortion of the CLC periodic structure into a, low efficiency, rectangular profile, with a worsening of the DFB mechanism; thus, a decrease in the lasing intensity is observed. By further increasing the field, the CLC helix completely unwinds and the structure becomes Nematic: the DFB effect can no more take place and all microlasers are switched off.



Luciano De Sio *et. al*

**Figure 30** Sketch of a microlaser array realized in a POLICRYPS structure.



Luciano De Sio *et. al*

**Figure 31** Emitted intensity and FWHM dependence on input pump energy. *Reproduced from Strangi et al. (2005).*

Figure 32 shows the spatial distribution of the laser emission emerging from the microcavities. The image is acquired by scanning with a high resolution CCD camera, in the proximity of the output edge of the sample, perpendicularly to the microchannels. The intensity profile indicates that maxima of lasing intensities have a spatial periodicity  $\Lambda_L \approx 5 \mu\text{m}$ , which almost coincides with the POLICRYPS pitch  $\Lambda$ . This circumstance confirms that the POLICRYPS microchannels act as a series of miniaturized

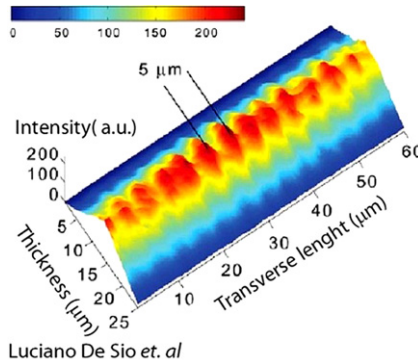


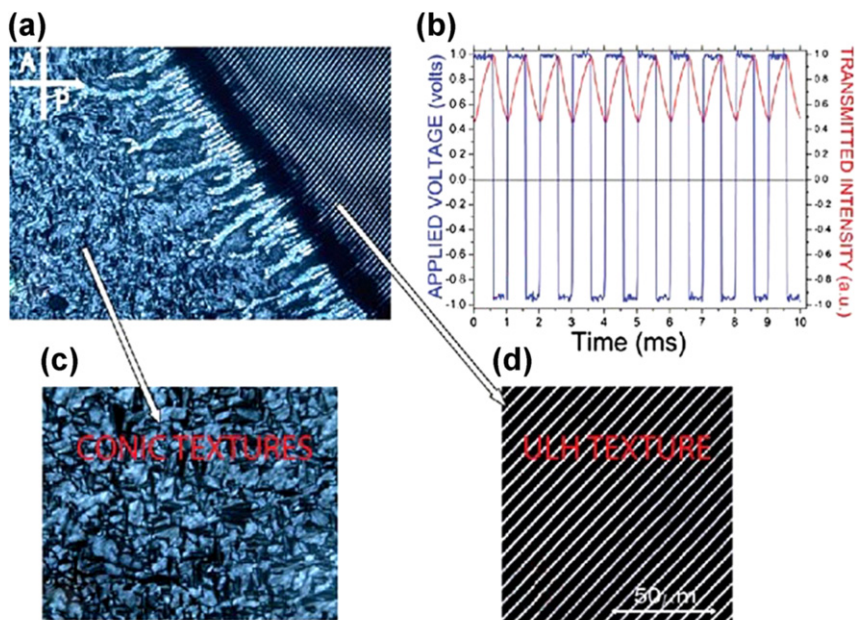
**Figure 32** Spatial distribution of the radiation emerging from the POLICRYPS channels. Reproduced from *Strangi et al. (2005)*.

mirrorless cavity lasers; in each of them, the emitted laser lights propagate along the CLC helical axes, which behave as Bragg resonators. Finally, it has been also shown that, in this kind of system, the emitted laser wavelength  $\lambda_L$  can be tuned by varying the sample temperature: from 25 to 80 °C, a tuning of  $\lambda_L$  is obtained, with an average red-shift of 0.2 nm/°C, in the spectral range 580–590 nm. Indeed, the pitch  $p$  of the CLC increases with temperature (Blinov, 1983), with a consequent red-shift of the stop-band edge, where lasing takes place.

#### 4.3.2 CLC in ULH Configuration

In a short pitch CLC film, whose helical axis is uniformly aligned in the plane of two confining substrates (the Uniform Lying Helix texture, ULH), an in-plane rotation of the axis is obtained by applying an electric field across the film: it is the “Flexo-Electro-Optic effect” (FEO) (Patel & Meyer, 1987). Applications based on this effect present some technical drawback; in particular, a warm up voltage is required to maintain the CLC in the ULH configuration. Recently, an “empty POLICRYPS template” has been exploited to induce the ULH configuration in a short pitch CLC (BL088, helixpitch  $\sim 400$  nm) (Carbone et al., 2009). Figure 14a shows a POM view of the sample at the edge of the grating area; on the left, a typical focal conic texture can be recognized, which is induced by a random distribution of the helical axes (high magnification in Figure 33c). On the right, a ULH geometry, induced by the POLICRYPS structure, is well evident (high magnification in Figure 33d). Electro-optical features are studied by utilizing a sample thickness ( $L = 10$  μm) which maximizes light transmission.





Luciano De Sio et. al

**Figure 33** POM view of the POLICRYPS template filled with CLC at the of grating area edge (a). High magnification of the CLC randomly oriented (c), and in ULH geometry (d); its electro-optical response (b). *Reproduced from De Sio, Ferjani, et al. (2011).*

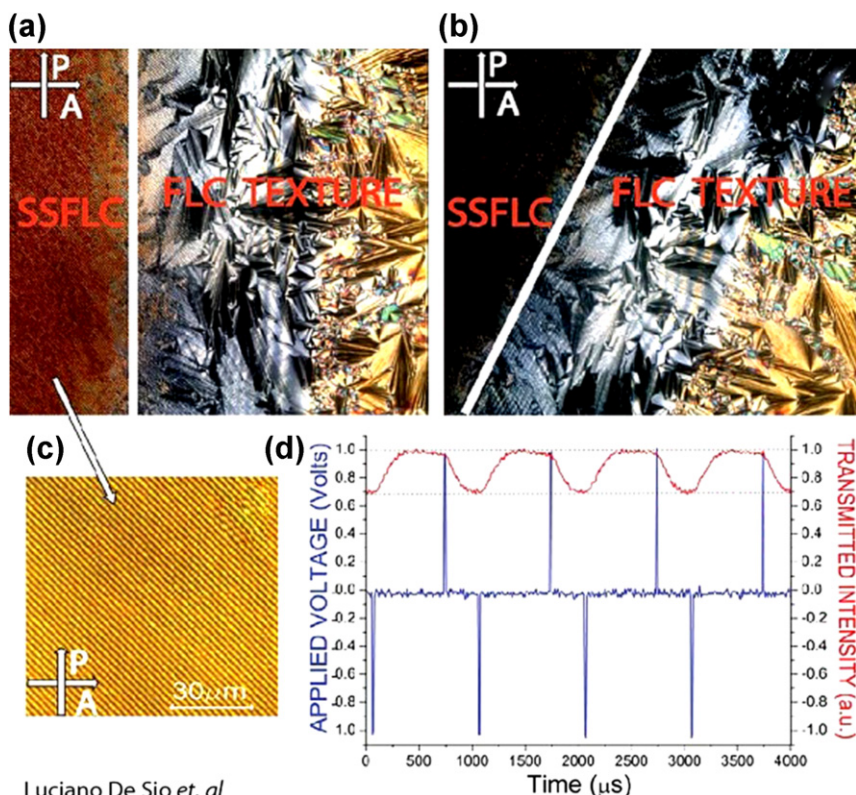
Application of an external field (1 kHz square wave, Figure 33b) across the cell, in the area of Figure 33d, induces an in-plane tilt of the CLC optical axis; the tilt is inverted if the polarity of the electric field is reversed. The transmitted intensity (red curve<sup>1</sup> in Figure 33b) depends on the tilt of the optical axis (Carbone et al., 2009), which is proportional to the applied field (Hegde & Komitov, 2010). The response is therefore linear with the applied field (up to  $6.3 \text{ V}/\mu\text{m}$ ), with characteristic times that are in the  $\mu\text{s}$  range (De Sio, Ferjani, et al., 2011).

#### 4.3.3 SSFLC Switching

FLCs, exhibit a permanent polarization (Meyer, 1969) and can be utilized for the realization of the so-called “Surface Stabilized Ferroelectric Liquid Crystal” (SSFLC) (Clark & Lagerwall, 1980) arrangement. Devices based on this configuration exhibit a fast response, a wide view angle and a bistable

<sup>1</sup> For interpretation of color in Figures 33, 34, 41, and 43, the reader is referred to the web version of this book.





Luciano De Sio et. al

**Figure 34** POM view of the template (grating vector at 45° with the polarization direction) filled with FLC at the grating area edge (a) and after rotating the grating vector of 45° (b). The bistable response of the depicted area (c) is reported in (d). *Reproduced from De Sio, Ferjani, et al. (2011).*

memory capability and are promising from an application oriented point of view; their real performances, however, can be affected by technical problems, mainly concerned with the need of mechanical stability. In this framework, the “empty POLICRYPS template” has been used to align FLCs; results, obtained by injecting CS-1024 FLC in a cell of  $L = 10 \mu\text{m}$  thickness and  $\Lambda = 3 \mu\text{m}$  pitch, are shown in Figure 34 (De Sio, Ferjani, et al., 2011). A POM view of the sample at the edge of the grating area shows the typical focal conic texture of randomly aligned FLC molecules (right view, Figure 34a and b), while a uniaxial plate can be recognized in the grating area (left view, Figure 34a and b).

A 45° rotation of the sample in the POM shows that the randomly aligned FLC region (right) remains almost unchanged, while the SSFLC

area (left) becomes dark, thus indicating that a director alignment takes place only in this region. Indeed, due to the boundary conditions imposed by the polymeric slices, the molecular director sets at an angle of  $22^\circ$  with the normal to them. The electro-optical effect is obtained by applying a voltage that switches the director orientation ( $\pm 22^\circ$ ); as a consequence, also the polarization axis (perpendicular to the molecular director) is switched between two stable states (Clark & Lagerwall, 1980). Figure 34d shows this bistable behavior as observed in the intensity transmitted by the SSFLC area (Figure 34c), obtained by applying a bipolar electric pulse with a 1 ms period (blue curve, Figure 34d).



## 5. TUNABLE DIFFRACTIVE WAVEPLATES

### 5.1 The New Generation of Optics

In addition to refractive index and shape of a material, there is one more key parameter that efficiently controls with propagation of light the orientation of the optical axis of a birefringent materials. Thin films of such materials are widely used for changing retardation between polarization components of a light beam thus changing polarization of a beam. Most important among them are the half-wave plates that allow rotating polarization of light, or converting it to a circular and vice versa. An incident linearly polarized light emerges from such waveplate maintaining its linear polarization state, however, having it rotated double the angle made between the polarization direction and the optical axis of the waveplate. A circularly polarized incident light emerges from a half-wave plate with reversed handedness of the polarization. The effect of the angle  $\alpha$  of the optical axis of the waveplate is exhibited by a phase shift,  $\Phi = 2\alpha$ , that is determined by the angle only and does not depend on wavelength (Tabiryan, Nersisyan, Steeves, & Kimball, 2010). Advances in LC materials and technology allow fabricating waveplates wherein the optical axis orientation is patterned and even continuously modulated in space,  $\alpha = \alpha(x, y)$ . In a simplest realization,  $\alpha$  is a linear function of coordinate, Cartesian ( $x$ ),  $\alpha = qx$  or polar ( $\varphi$ ),  $\alpha = q_\varphi\varphi$  (Figure 35). The wavevectors  $q = \pi/\Lambda$  and  $q_\varphi = n/2$  ( $n = \pm 1, 2, \dots$ ) determine the period of the pattern with  $\Lambda$  representing the pitch of so-called cycloidal pattern, and  $n$  known as the charge number of the singularity of the axial modulation of optical axis orientation.

Thus, these optical structures are diffractive optical elements, diffractive waveplates (DW), that impose a phase modulation pattern  $\Phi = \pm 2\alpha(x, y)$  on circular polarized beams depending on the handedness of polarization.

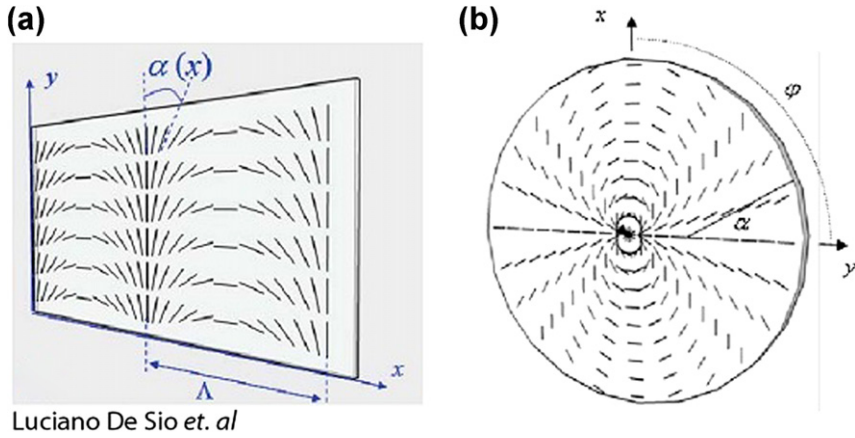


**Figure 35** 1D patterns of optical axis orientation in a half-wave plate: (a) cycloidal and (b) azimuthal.

Note that the phase modulation of a circular polarized beam at the output of a “Cycloidal” DW (CDW),

$$\mathbf{E}_{\text{out}} = \mathbf{E}_{\text{in}} e^{2i\alpha(x,y)} = \mathbf{E}_{\text{in}} e^{\pm 2iqx} \quad (1.10)$$

corresponds to  $\pm 1$ st order diffracted beams, depending on the polarization sign in the input beam, having diffraction efficiency:

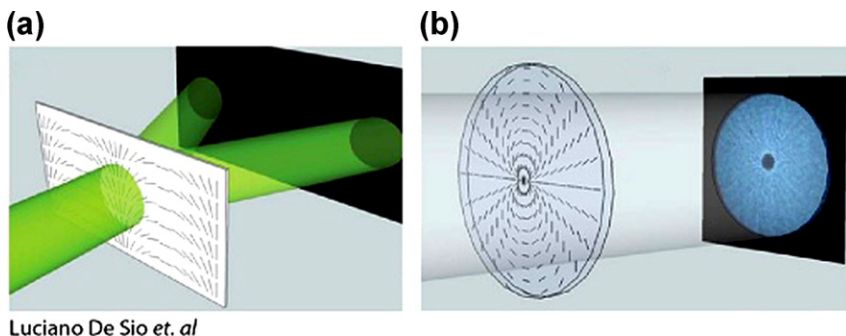
$$\eta = \sin^2 \frac{\pi L(n_e - n_o)}{\lambda}, \quad (1.11)$$

where  $L$  is the thickness of the waveplate, and  $n_e, n_o$  are the principal values of refractive indices. Thus the maximal diffraction occurs at the wavelength meeting the half-wave phase retardation condition  $\lambda = 2L(n_e - n_o)$ . Vortex beams are generated for a waveplate with axial symmetry (ADWs) as reported in Figure 36:

$$\mathbf{E}_{\text{out}} = \mathbf{E}_{\text{in}} e^{2i\alpha(x,y)} = \mathbf{E}_{\text{in}} e^{\pm 2in\phi}. \quad (1.12)$$

Since the phase  $\Phi$ , otherwise known also as geometrical phase or Pancharatnam phase (Bhandari, 1997), does not depend on wavelength, these diffractive components are naturally broadband.

Even if anisotropic thin structures ( $\sim 1 \mu\text{m}$ ) with ability of 100% transmission modulation were known and suggested for LCD application a decade ago, see the review papers (Nersisyan, Tabiryan, Steeves, & Kimball, 2009; Tabiryan et al., 2010) the technology of their fabrication in good quality



Luciano De Sio *et. al*

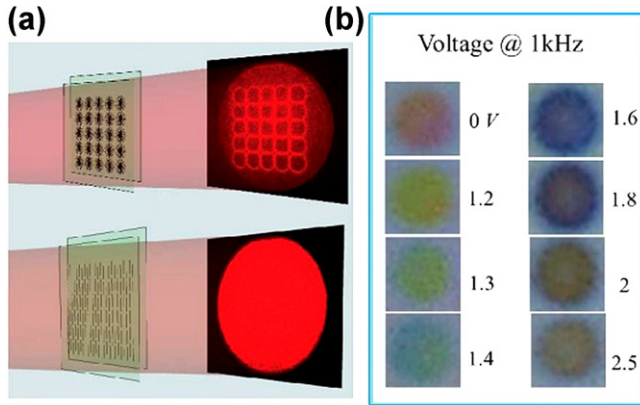
**Figure 36** Cycloidal (a) and azimuthal (b) ADWs transform an input beam into a "doughnut" beam. The angular size of the "doughnut" can be increased by increasing the vortex degree  $n$ .

over a reasonably large area was developed only recently both for so-called CDWs, known also as polarization gratings, as well as for waveplates with axial modulation of LC orientation (ADWs), known also as vortex waveplates. The printing technique for fabricating these DWs utilizing linear-to-cycloidal and axial polarization converters is inexpensive, robust against mechanical and ambient noise, and allows volume production of larger area components. It also allows producing DWs with doubled spatial frequency of LC orientation modulation.

## 5.2 Light Modulation Concepts Based on DWs

The diffraction spectrum of DWs can be controlled by varying the optical anisotropy of DWs. Using azo-LC and LC polymer-based CDWs, complete switching between diffractive and non-diffractive states was demonstrated for CW radiation as well as for nanosecond pulses due to vanishing optical anisotropy (Nersisyan *et al.*, 2009). The diffraction of DWs can be controlled and switched also electrically, due to reorientation of LC between the spatially modulated diffractive and homogeneous non-diffractive states.

Figure 37a shows an example of such switching for a high order LC ADW array (Nersisyan, Kimball, Steeves, & Tabiryan, 2010). Using white light illumination, the transmission spectrum of individual pixel elements can be tuned to different wavelengths with a rather small variation of voltage (Figure 37b). A disadvantage for certain applications is the circumstance that the state of DWs at the absence of external stimuli is diffractive, and the transmittive state requires application of voltage, a light beam, or another



Luciano De Sio et. al

**Figure 37** A “doughnut” pixel in an array (a) can be switched between on (bright) and off (dark) states, reversibly, with application of a small voltage ( $\sim 1$  V) and with a high contrast ratio (b).

stimulus. Combination of two DWs, however, was shown to allow canceling the effect of diffraction, and a light beam, even a white light beam, may propagate through such a system without attenuation or distortion if broadband/achromatic DWs are in use.

The input CDW splits an unpolarized light into two beams, right- and left-circularly polarized (Figure 38a) while the second CDW at parallel arrangement restores collinear propagation without introducing appreciable lateral shift due to thinness of adjacent CDWs. The Switching of the diffraction of one of the CDWs results can be used as a diffractive output (Figure 38b). Switching complex orientation patterns is not always desirable, and can be replaced by switching the polarization states instead using a LC phase retarder. The concept of switching using optically controlled phase retarder based on azobenzene LC is shown in Figure 39.

Thus, DWs present unique advantages for photonics due to their thinness, hence reduced losses, high efficiency, broadband nature, feasibility of polarization independent functionality, and the technological opportunity to produce DWs in the form of thin film coatings on desired substrates. Note that a wide range of azobenzene LC materials have been developed for using CW as well as short laser pulses for all-optical control (Hrozhyk et al., 2010). In an ultimate realization, the diffractive properties of CDWs were combined with reflective properties of CLCs to realize a variable transmission-to-reflection switching system using a conventional LC phase retarder.

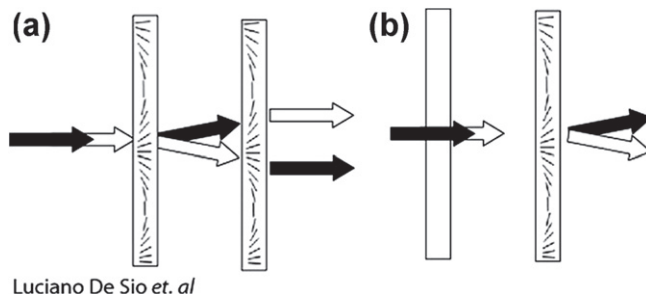


**Figure 38** Controlling the diffraction of CDWs (a). Switching of the diffraction of one of the CDWs results in a diffractive output (b). Black and white arrows correspond to right- and left-circular polarized beams.

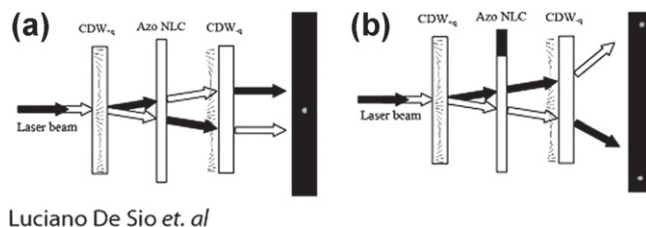


**Figure 39** A planar aligned LC cell acting as a half-wave plate between anti-parallel CDWs reverses the handedness of the beams leading to overlapping collinear propagating output (a). Photoinduced isothermal phase transition from the nematic to isotropic phase eliminates the birefringence of the azo NLC thereby disrupting the polarization converting ability of the azo NLC waveplate resulting in doubled diffraction angle between the beams. Black and white arrows correspond to right- and left-circular polarized beams, respectively (b).

## 6. LIQUID CRYSTALS ACTIVE PLASMONIC NANOMATERIALS

### 6.1 General Overview

Nanomaterials possess a very small feature size (1–100 nm) and can be metals, polymers, or even composite materials. They have the potential for wide-ranging industrial, medicine, and electronic applications; in particular, noble metal nanoparticles are of great interest because of their tunable absorption and scattering resonances caused by collective oscillations of the conduction band electrons, the so-called Localized Surface Plasmon (LSP). The plasmonic coupling between these nanoparticles and light localizes visible light into a nanometer-sized volume and is at the basis of a range of interesting



optical phenomena, such as Surface Enhanced Raman Spectroscopy (SERS), Resonance Light Scattering (RLS), and Surface Plasmon Resonance (SPR). Controlling the spectral position of the LSP resonance is therefore a hot topic and different approaches have been experimented to realize this goal. The possibility of varying both size and shape of the utilized particles reaches the aim, but, necessarily, only samples with static properties can be realized in this way. An interesting alternative exploits the high sensitivity of LSP to the dielectric constant of the surrounding media (Kossyrev et al., 2005); in this framework, the large anisotropy of the refractive index of LCs enables tuning the LSP by acting on the LCs with some external perturbation (electric and optical field, temperature, etc.). A first attempt (Kossyrev et al., 2005) reports on the realization of a layer-by-layer structure composed by an array of gold nanoparticles (GPNs) alternated to a NLC film: by applying an external electric field to the sample, a LSP red-shift of about 8 nm has been observed. In different approaches, a self-organization of gold nanorods is imposed by an intrinsic cylindrical micelle self-assembly, which takes place both in NLCs and hexagonal LCs (Liu, Cui, et al., 2010) while E-Beam lithography is exploited to realize a uniform gold nanodisk array covered with a dual frequency NLC, which controls the LSP response (Liu, Hao, et al., 2010). However, a drawback in the use of LCs is represented, in general, by the need of chemical and/or mechanical treatments that ensure a director alignment; in addition, the order degree of LCs is affected by the inclusion of nanoparticles and therefore their concentration in the host LC must be limited to a few percent. To overcome these difficulties, a new approach has been recently utilized, which yields a self-organization of CLCs infiltrated in a micro-periodic polymeric template and, then, a nanoscale organization of GNPs (De Sio, Caputo, Cataldi, & Umeton, 2011). In a further experiment, the technique enables a twofold active control of the plasmonic resonance of randomly distributed GNPs (De Sio et al., 2012).

## 6.2 Periodic Structures Hosting Plasmonic CLCs

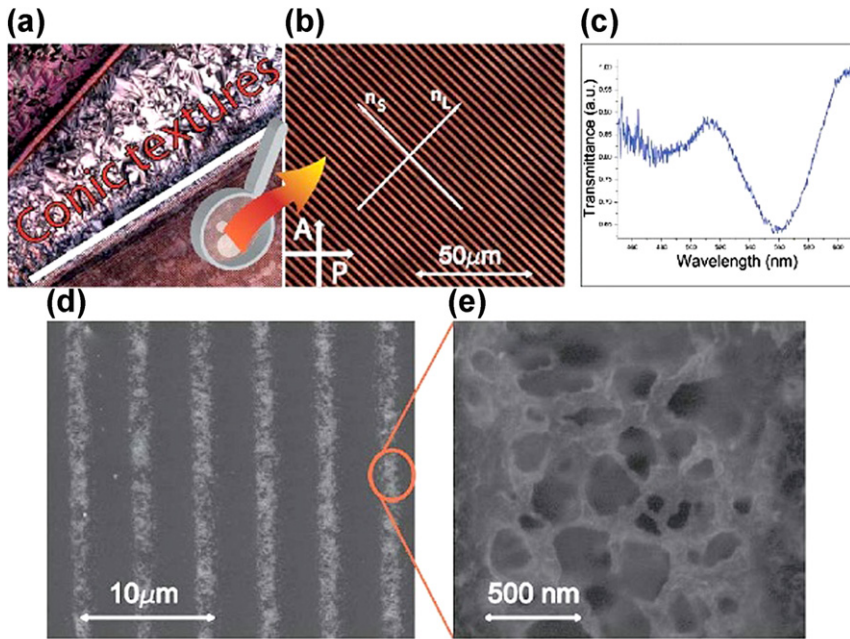
The already described “empty POLICRYPS” platform (De Sio, Ferjani, et al., 2011) has been recently utilized for efficiently aligning CLC doped with GPNs. The BL095 CLC (helix pitch  $\sim 400$  nm) mixed to the Harima Gold nanopaste NPG-J, which contains 55 wt% of GNPs. These exhibit an average diameter of about 10 nm and a plasmonic absorption peak in solvent (naphthen) at  $\lambda = 525$  nm; the capping agent utilized to avoid clustering of GNPs is not known, being the NPG-J nanopaste a patented commercial product. However, the material is liquid at room temperature and, when



diluted in Chloroform, it shows a dark red coloration, strong indication of a mono-dispersion of GNPs. These are mixed to the CLC in high concentration ( $\sim 20$  wt%) and then infiltrated, by capillarity, in the polymeric template; the sample is kept at a fixed high temperature ( $\sim 90$  °C) during the whole filling process, thus allowing the CLC to remain in the isotropic phase. When cooling down the sample to room temperature, a self-organization process occurs, which orients the CLC helices parallel to the polymeric slices, in a Uniform Lying Helix (ULH) configuration (Carbone et al., 2009). The best performances are exhibited by a grating of  $L = 10$   $\mu\text{m}$  thickness and  $\Lambda = 6$   $\mu\text{m}$  pitch. Figure 40a is a POM micrograph of the sample at the edge of the grating area. The standard focal conic texture on the left is due to a random distribution of the helical axes; on the right, the polymeric structure induces a ULH geometry (Figure 40b), confirmed by the detection of a spectral stop band, typical of a short pitch CLC (Figure 40c). The high magnification in Figure 40b shows that, despite a high GNP concentration, the CLC exhibits a uniform alignment of organized helices, confined between polymeric slices. This is an indication of good “host-fluidity” properties of the CLC for GNPs; at the same time, the high degree of order of the CLC indicates that this phase is only weakly perturbed by the GNPs. Realization of the described structure represents a successful combination of “top-down” approach (template fabrication) with a “bottom-up” one, that is the self-organization of GNPs inside the CLC helices.

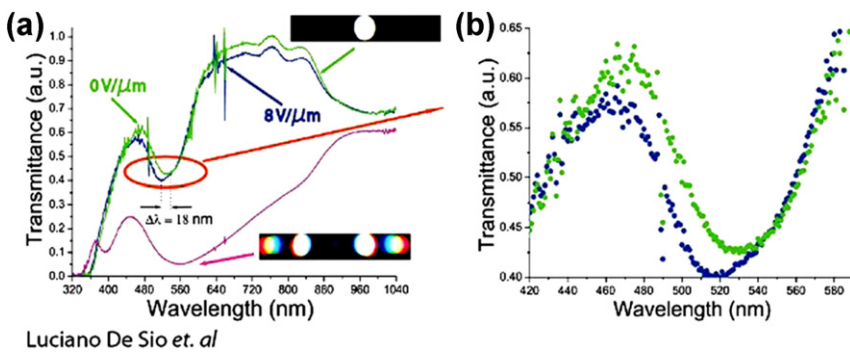
The distribution of Au NPs within the CLC has been studied both with a Scanning Electron Microscope (SEM) and an Electron Back-Scattering Diffraction (EBSD), an analysis that enables distinguishing Gold from other materials, since the yield of backscattered electrons increases with the specimen atomic number ( $Z$ ); in the actual case, the presence of Gold ( $Z = 79$ ) produces a high contrast with the polymer microstructure (a thiol based system with  $Z \sim 18$ ). The bright stripes of Figure 40d confirm the presence of Au along the microchannels only, while in the high magnification (Figure 40e), CLC branches are “wrapped” by densely packed Au NPs, whose morphological details cannot be shown with the actual SEM resolution, due to their small average size ( $\sim 10$  nm). The spectral response of the structure is investigated by probing the sample with linearly polarized white light at normal incidence; results are reported in Figure 41.

While p-polarized light is strongly diffracted and its transmission is almost suppressed (Figure 41a, magenta curve), s-polarized light is highly transmitted in almost the whole analyzed range (Figure 41a, blue curve). This behavior, already observed in the past (Strangi et al., 2005), can be explained



Luciano De Sio et. al

**Figure 40** POM view of the polymeric template filled with CLC and GNPs mixture at the edge of the grating area (a). The high magnification of the area aligned in ULH geometry is shown in (b) while its typical reflection notch is reported in (c). EBSD view (d) and high magnification (e) of the polymeric template filled with CLC and GNPs. *Reproduced from De Sio, Caputo, et al. (2011).*



Luciano De Sio et. al

**Figure 41** Spectral response of the sample for two values of the external electric field (a) and its higher magnification detail (b). *Reproduced from De Sio, Caputo, et al. (2011).*

by supposing that CLC helices lay, in average, along the channels of the template structure; thus, two different effective refractive indices exist:  $n_{\perp}$  (estimated  $\sim 1.64$ ), quite different from the polymeric refractive index  $n_p$  ( $\sim 1.54$ ), which is experienced by light whose electric field is perpendicular to the channels (p-wave), and  $n_{\parallel}$  (estimated  $\sim 1.56 \sim n_p$ ) for light whose electric field is parallel to them (s-wave). The alternation of  $n_{\perp}$  and  $n_p$  indices (the grating structure) is therefore experienced only by the p-wave. In the blue curve of Figure 41a, a pronounced absorption peak at  $\lambda = 532$  nm, with an extinction coefficient of 0.2 is observed, which cannot be attributed to any diffractive mechanism, since the sample appears optically homogeneous ( $n_{\parallel} \sim n_p$ ) to the incoming s-wave. Both the spectral position and the narrow width of the measured peak suggest, instead, that it is due to the LSP of GNPs dispersed in the CLC, an hypothesis supported by similar results reported in literature (Kossyrev et al., 2005), and observed in different systems where GNPs are also involved (Link & El-Sayed, 1999). The observed plasmonic response is also tunable, as demonstrated by applying an external electric field ( $8 \text{ V}/\mu\text{m}$ , 1 kHz, square wave) across the cell, perpendicularly to the helix axes. In fact, this field induces an in-plane tilt of the optical axis of the CLC, with a consequent variation of the  $n_{\parallel}$  refractive index, experienced by the s-wave. This index variation drives the plasmon resonance frequency. Indeed, the optical behavior of a spherical particle dispersion is described by the Mie theory (Mie, 1908) through the extinction coefficient:

$$\sigma_{\text{ext}}(\omega) = 9 \frac{\omega}{c} \varepsilon_m^{3/2} V_0 \frac{\varepsilon_2(\omega)}{[\varepsilon_1(\omega) + 2\varepsilon_m]^2 + \varepsilon_2(\omega)^2}, \quad (1.13)$$

where  $V_0 = (4\pi/3)R^3$  is the nanoparticles volume,  $R$  being its radius, and  $\omega$  is the angular frequency of the impinging radiation;  $\varepsilon_m$  is the dielectric function of the medium surrounding the nanoparticles, and  $\varepsilon_1$  and  $\varepsilon_2$  are the real and imaginary parts of the nanoparticle dielectric function, respectively. Thus, for small and isolated metal particles, the spectral position of the plasmonic absorption peak depends on the refractive index of the surrounding medium, according to the condition that minimizes the denominator of Equation (1.13):

$$\varepsilon_1(\omega) = -2\varepsilon_m. \quad (1.14)$$

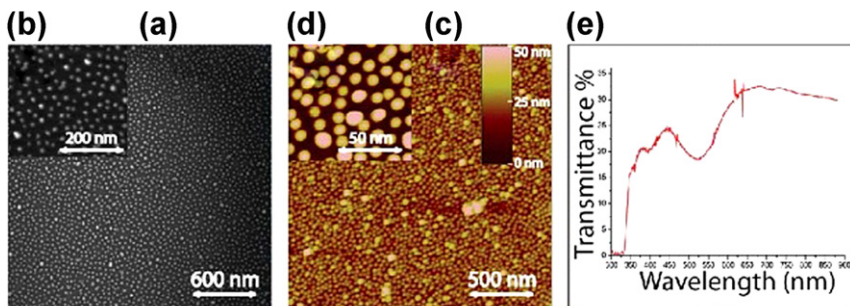
A modification in the dielectric function of the host material corresponds, therefore, to a tuning action of the plasmon resonance frequency. In the actual case, when applying the external electric field, the impinging light experiences a decreased value of the CLC refractive index (from  $n_{\parallel}$  to  $\sim n_o$ ); following Equation (1.14), the resonance condition is fulfilled for higher

(negative) values of  $\varepsilon_1(\omega)$ . Since, in the visible range, the real part of the electric permittivity of GNPs increases with frequency (Johnson & Christy, 1972), fulfillment of Equation (1.14) takes place for higher values of  $\omega$ ; this yields a blue-shift of the plasmonic absorption peak. This is confirmed by results shown in Figure 2b (higher magnification of the highlighted region of Figure 2a): the absorption peak is blue shifted from  $\lambda = 532$  nm (blue curve Figure 41b) to  $\lambda = 514$  nm (red curve Figure 41b). An additional tunability of the plasmonic response of the composite structure is obtained by varying its temperature. When this is increased from 25 up to 75 °C, a red-shift of the plasmonic absorption peak is observed in the range 532–582 nm. This behavior can be explained in terms of a temperature induced passage from densely packed to mono-dispersed GNPs. Indeed, the pitch  $p$  of a CLC elongates with temperature (Blinov, 1983); assuming that the CLC helices are wrapped by GNPs, the consequence of this elongation is an increase of the inter-distance between neighboring metal NPs. It has been demonstrated that the plasmon response of NP arrays depends on particle size and density; results show that, for densely packed metal NPs, the absorption peak is quite broad and is centered in the blue–green range, while this peak slightly reduces its width and shifts to the red in case of well separated NPs (Kinnan & Chumanov, 2010).

### 6.3 Random Distribution of GNPs Layered with NLC

Realization of large area layered arrays of GPNs, obtained by combining bottom-up and self-assembly processes, without the need of any particular nanotechnology facility, represents a step-forward in comparison with similar approaches reported in literature (Cunningham, Mühlig, Rockstuhl, & Bürgi, 2011). Large-scale ( $\sim\text{cm}^2$ ) GNP arrays are immobilized on a conductive substrate layered with an NLC film, used as “active” surrounding medium. Characterizations reported in the following refer to two GNP arrays separated by seven polyelectrolyte layers, while the SEM image refers to a single GNP array.

In this image (Figure 3a and b) GNPs appear well dispersed and approximately equally spaced with an average radius of  $\sim 10$  nm; they are randomly distributed and no kind organization can be discerned. The Atomic Force Microscopy (AFM) topography of the two GNP arrays reported in Figure 42c and d confirms this result: The analysis (color scale, Figure 42c) shows an average radius of about 15 nm with a modulation depth of 22 nm; the discrepancy in the measured radius between the SEM and AFM characterization is due to the convolution between the AFM tip and the average size



Luciano De Sio *et. al*

**Figure 42** SEM view (a) and its high magnification (b), AFM topography (c) and its high magnification (d) of the GNPs distribution. Spectral response of the sample (e). Reproduced from *De Sio et al. (2012)*.

of the GNPs, which are of the same order of magnitude, while, due to the high vertical resolution ( $\sim 0.1$  nm), the modulation depth is an accurate measurement of the intra-layer distance. The spectral response of the GNP arrays is investigated by probing the sample with unpolarized white light impinging at normal incidence. In Figure 42e, a pronounced absorption peak at  $\lambda = 522$  nm, with a measured extinction coefficient of  $\sim 10\%$ , is shown. Both the spectral position and the narrow width of the peak confirm the existence of a LPR of well dispersed GNPs (Kossyrev *et al.*, 2005). For the realization of an active control of the plasmonic resonance, a glass cell is fabricated by combining the substrate containing GNP layers with a conductive cover glass, treated with a thin polyimide layer for inducing a planar alignment of the NLC director. Glass and GNP-coated substrates are kept at a controlled distance by  $4 \mu\text{m}$  glass microspheres; the NLC in the isotropic phase ( $65^\circ\text{C}$ , E7) is introduced by capillarity. A good NLC alignment is realized by slowly cooling down the sample to room temperature through a low-slope linear ramp (De Sio, Ferjani, *et al.*, 2011).

In the bulk of the cell, the NLC director exhibits a hybrid configuration due to a competition between a homeotropic alignment, induced by the electrostatic interaction (Kossyrev *et al.*, 2005) with GNPs on one side of the cell, and the planar alignment induced by the functionalized top cover glass on the other side (Figure 43a). Electro-optical experiments are carried out by putting the sample between crossed polarizers, with its director axis (red arrow Figure 43a) placed at  $45^\circ$  with respect to the polarizer/analyzer axes, and monitoring the transmitted intensity of a monochromatic light (He-Ne laser,  $\lambda = 633$  nm) while applying an external field  $E_{ext}$  (1 kHz,

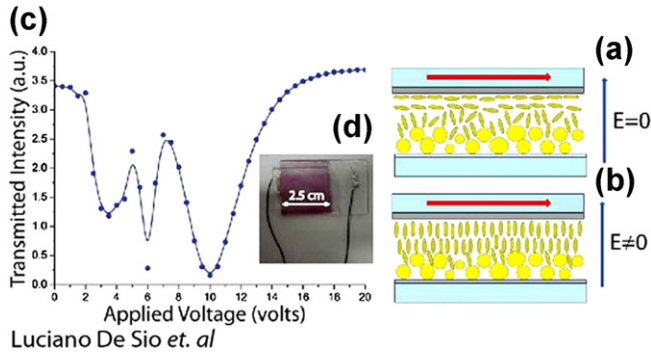
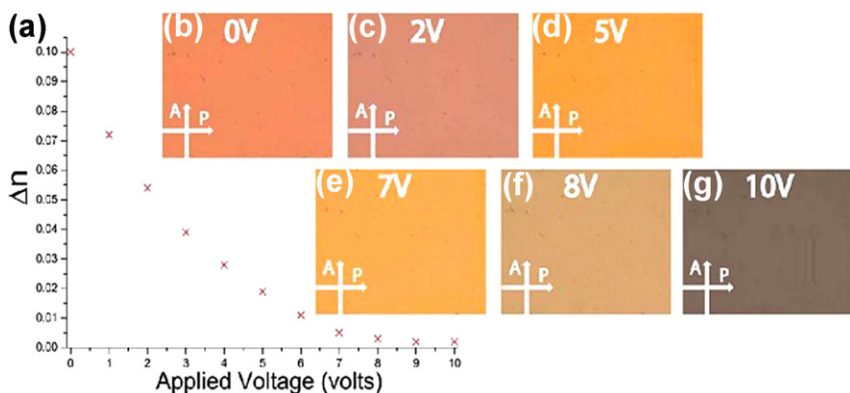


**Figure 43** Electro-optic response (c) of the large area ( $1 \text{ cm}^2$ ) sample (d) with a hybrid NLC configuration. Sketch of the NLC configuration inside the cell without (a) and with (b) application of an external electric field. *Reproduced from De Sio et al. (2012).*

square wave). The oscillating behavior reported in Figure 43c recalls the optical response of a planar aligned LCs cell, whose transmittivity between crossed polarizers is related to its birefringence. This one depends on the presence of external fields and on sample temperature (Wu, Efron, & Hess, 1984); under the influence of an applied electric field, the NLC director reorients along the field direction, thus changing the effective birefringence of the device and modulating the transmitted light intensity. In the actual case, however, due to the presence of a hybrid alignment, the formalism used in Wu et al. (1984) cannot be used to quantitatively explain the behavior reported in Figure 43c. In any case, the initial birefringence of the hybrid cell, responsible for the observed behavior, is directly measured by means of an optical compensator and holds  $\Delta n \sim 0.10$  (typical value in a hybrid NLC cell); then, due to the induced director reorientation, this value is varied, and eventually switched to zero, by increasing  $E_{ext}$ .

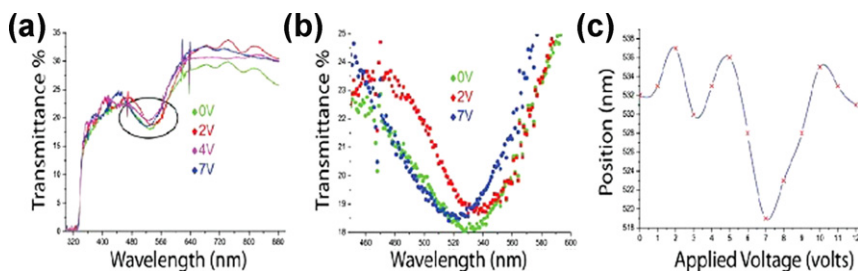
Observations with the POM, equipped with a CCD color camera connected to a PC (Figure 44b–g), show that the whole area changes contrast uniformly, suggesting both that  $E_{ext}$  is applied uniformly over the whole sample, and that the NLC director alignment is not affected by the presence of GNPs (eventually removed from the layer, that might give rise to NLC defects). Thus, observations confirm that GNPs are well immobilized on the glass substrate. The influence of  $\Delta n$  variation on the plasmonic resonance of the GNP array is investigated by detecting, for different values of  $E_{ext}$ , the spectral response of the sample when probed with unpolarized white light at normal incidence ( $\lambda$  in the range 300–900 nm). Figure 45a shows that, by increasing  $E_{ext}$ , the LPR absorption peak exhibits a “dancing behavior,”





Luciano De Sio *et. al*

**Figure 44** Birefringence variation versus the applied electric field (a). POM view of the sample while increasing the applied electric field (b–g). *Reproduced from De Sio et al. (2012).*



Luciano De Sio *et. al*

**Figure 45** Spectral response of the sample for different applied voltages (a) and its higher magnification detail (b). Position of the center of the plasmonic resonance versus the applied voltage (c). *Reproduced from De Sio et al. (2012).*

with a continuous blue–red shift of its position (well evident in the high magnification of Figure 45b). This is in contrast with predictions of the Mie theory (Mie, 1908), which yields the expression reported in Equation (1.13).

In that framework, from Equations (1.13) and (1.14), a monotonic dependence of the LPR wavelength on the refractive index of the surrounding medium is expected; thus, in the actual case, a decrease of the NLC refractive index value (roughly estimated from  $\sim 1.6$  to  $\sim 1.5$ ), obtained under the influence of  $E_{ext}$ , should yield a monotonic blue-shift of the LPR wavelength. The observed unusual non-linear modulation of this shift (Figure 45c) might be explained by taking into account also the influence of the ITO



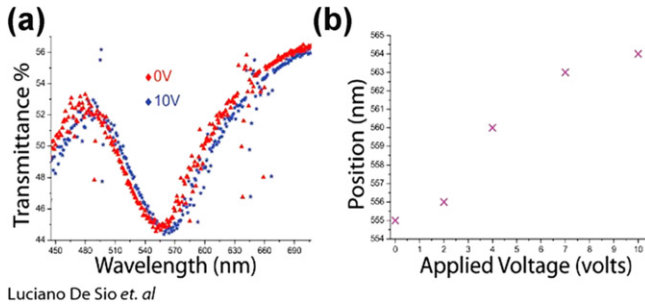


**Figure 46** Spectral response of the empty sample (a) and plasmonic resonance wavelength (b) versus the applied external field. *Reproduced from De Sio et al. (2012).*

layer underlying the GNP array. Indeed, it has been recently demonstrated (Feigenbaum, Diest, & Atwater, 2010) that unity-order refractive index variations can be induced by the presence of free carrier accumulation layers, an effect which takes place when an external electric field is applied to a system of ITO and GNPs layers separated by a dielectric one ( $\text{SiO}_2$ , in the case of Feigenbaum et al. (2010)). It is worth noting that no refractive index variation is observed unless the  $\text{SiO}_2$  layer is present. Because of the organosilane layer used to functionalize the glass/ITO substrate (Cunningham et al., 2011) the actual system is similar to the one described in Feigenbaum et al., 2011; thus, it can be expected that, also in this case, the formation of a free carrier accumulation layer at the organosilane/ITO interface takes place, which can induce a refractive index variation on field application. That is to say, this layer behaves as an additional “active” medium. This hypothesis is verified by an electro-optical experiment in which the NLC of the sample has been substituted by air. Results are reported in Figure 46a and b: By increasing  $E_{ext}$ , from 0 to  $2.5 \text{ V}/\mu\text{m}$ , only a monotonic red-shift of about 9 nm is observed, which confirms both the role played by the organosilane in the glass/ITO substrate in creating a free carrier accumulation layer and the validity of the Mie model for the GNPs.

Figure 45c suggests, therefore, that, under the influence of the external electric field, the free carrier accumulation and the NLC layers enter somehow in competition as “active” media surrounding the GNPs. The way they contribute to determine the spectral position of the is not yet clear; probably, depending on the value of  $E_{ext}$ , they combine their effects in a different way, thus causing either an increase or a decrease of the effective refractive index of the medium surrounding the GNPs, which corresponds to the observed “dancing behavior” of the LPR wavelength (Figure 45c).



## 7. CONCLUSIONS

In conclusion of this review we can assert that unique optical properties and capabilities of LCs have been successfully applied, in the last years, in a wide variety of applications. It has been demonstrated that electro- and photo-responsive CLCs enable fabrication and enhance capabilities of photonic devices. Polymeric-LC composite structures like Holographic Polymer-Dispersed Liquid Crystals allow realization of unequaled switchable reflection gratings, while self-aligning POLICRYPS structures were utilized as templates for complex materials, and for designing new generation of switchable photonic devices that include high quality transmission gratings, Bragg filters, polarizers, active phase retarders, and arrays of microlasers. A new generation of LC-based tunable diffractive waveplates open opportunities for new light modulation concepts. LCs doped with nanoparticles were exploited to obtain “active plasmonics” effects.

In all above applications, the superior performance exhibited by new generation of photonic devices proves LCs as the materials of choice for future. It is not fanciful to imagine that the obtained results may have a high social impact, by leading to efficient exploitation of solar energy, lighting, by helping to increase data capacity and the speed of optical communication systems and dynamically reconfigurable networks.

## ACKNOWLEDGMENTS

We acknowledge the cooperation of all co-authors of the papers we published on the argument: R. Bartolino, G. Strangi, R. Caputo, A. De Luca, A. Veltri, S. Ferjani, L. Pezzi, U. Cataldi, M.C. Tone, V. Verrina, G. Palermo, V. Caligiuri from the University of Calabria; G. Gilardi, R. Asquini, A. d'Alessandro, from Dipartimento di Ingegneria dell'Informazione, Elettronica e Telecomunicazioni, Sapienza Università di Roma; D. Donisi, R. Beccherelli, from Istituto per la Microelettronica e Microsistemi (CNR-IMM), Roma; A. Cunningham and T. Bürgi from the Université de Genève; U. Hrozhyk, S.R. Nersisyan, S. Serak, D. Steeves, R. Vergara, B. Ya. Zeldovich from Beam Engineering for Advanced Measurements Company, Orlando (USA); L.V. Natarajan and M. Rumi and long-standing support from AFRL/RX and AFOSR (C. Lee). The research leading to the reported results has received partial funding from: The US Air Force Office of Scientific Research (USAFOSR), Air Force Materiel Command (AFMC), US Air Force, under grant FA8655-12-1-003 (P.I. L. De Sio); The European Union's Seven Framework Programme (FP7/2007–2013) under grant agreement no. 228455.

## REFERENCES

- Abbate, G., Vita, F., Marino, A., Tkachenko, V., Slussarenko, S., Sakhno, O., et al. (2006). New generation of holographic gratings based on polymer-LC composites: POLICRYPS and POLIPHEN. *Molecular Crystals and Liquid Crystals*, 453, 1–13.

- Allahverdyan, K., & Galstian, T. (2011). Electrooptic jumps in natural helicoidal photonic bandgap structures. *Optics Express*, 19, 4611–4617.
- Anderle, K., Birenheide, R., Werner, M. J. A., & Wendorff, J. H. (2006). Molecular addressing—studies on light-induced reorientation in liquid-crystalline side chain polymers. *Liquid Crystals*, 33, 1421–1427.
- Atkins, P. W. (1987). *Physical chemistry*. Oxford: Oxford University Press.
- Bailey, C. A., Tondiglia, V. P., Natarajan, L. V., Duning, M. M., Bricker, R. L., & Sutherland, R. L. (2010). Electromechanical tuning of cholesteric liquid crystals. *Journal of Applied Physics*, 107, 013105/1–013105/8.
- Beckel, E. R., Natarajan, L. V., Tondiglia, V. P., Sutherland, R. L., & Bunning, T. J. (2007). Electro-optical properties of holographically patterned polymer-stabilized cholesteric liquid crystals. *Liquid Crystals*, 34, 1151–1158.
- Bhandari, R. (1997). Polarization of light and topological phases. *Physics Reports*, 282, 1–64.
- Blinov, L. M. (1983). *Electro-optical and magneto-optical properties of liquid crystals* (pp. 212–256). Chichester: Wiley.
- Blinov, L. M. (1996). Photoinduced molecular reorientation in polymers, Langmuir–Blodgett films and liquid crystals. *Journal of Nonlinear Optical Physics and Material*, 5, 165–187.
- Bowley, C., Fontecchio, A., Lin, J., Yuan, H., & Crawford, G. (1999). Advances in holographic polymer dispersed liquid crystal technology. *Materials Research Society Symposium Proceedings*, 559, 97–107.
- Bowley, C., Fontecchio, A., Crawford, G., Lin, J., Li, L., & Faris, S. (2000). Multiple gratings simultaneously formed in holographic polymer-dispersed liquid-crystal displays. *Applied Physics Letters*, 76(5), 523–525.
- Broer, D. J., Lub, J., & Mol, G. N. (1995). Wide-band reflective polarizers from cholesteric polymer networks with a pitch gradient. *Nature*, 378, 467–469.
- Broer, D. J., Mol, G. N., van Haaren, J. A. M. M., & Lub, J. (1999). Photo-induced diffusion in polymerizing chiral-nematic media. *Advanced Materials*, 11, 573–578.
- Bücher, H. K., Klingbiel, R. T., & VanMeter, J. P. (1974). Frequency-addressed liquid crystal field effect. *Applied Physics Letters*, 25, 186–188.
- Bunning, T., Natarajan, L., Tondiglia, V., Sutherland, R., Vezie, D., & Adams, W. (1995). The morphology and performance of holographic transmission gratings recorded in polymer dispersed liquid crystals. *Polymer*, 36(14), 2699–2708.
- Bunning, T., Natarajan, L., Tondiglia, V., Sutherland, R., Vezie, D., & Adams, W. (1996). Morphology of reflection holograms formed in situ using polymer-dispersed liquid crystals. *Polymer*, 37(14), 3147–3150.
- Bunning, T., Natarajan, L., Tondiglia, V., & Sutherland, R. (2000). Holographic polymer dispersed liquid crystals (H-PDLCs). *Annual Review of Materials Science*, 30, 83–115.
- Campbell, M., Sharp, D., Harrison, M., Denning, R., & Turberfield, A. (2000). Fabrication of photonic crystals for the visible spectrum by holographic lithography. *Nature*, 404(6773), 53–56.
- Caputo, R., De Sio, L., Sukhov, A. V., Veltri, A., & Umeton, C. (2004). Development of a new kind of switchable holographic grating made of liquid-crystal films separated by slices of polymeric material. *Optics Letters*, 29, 1261–1263.
- Caputo, R., Sukhov, A. V., Umeton, C., & Veltri, A. (2005). Kogelnik-like model for the diffraction efficiency of POLICRYPS gratings. *Journal of the Optical Society of America B*, 22, 735–742.
- Caputo, R., DeLuca, A., Sio, L., Pezzi, L., Strangi, G., Umeton, C., et al. (2009). POLICRYPS: A liquid crystal composed nano/microstructure with a wide range of optical and electro-optical applications. *Journal of Optics A: Pure and Applied Optics*, 11, 024017.
- Caputo, R., Trebisacce, I., De Sio, L., & Umeton, C. (2010). Jones matrix analysis of dichroic phase retarders realized in soft matter composite materials. *Optics Express*, 18, 5776–5784.

- Carbone, G., Salter, P., Elston, S. J., Raynes, P., De Sio, L., & Ferjani, S., et al. (2009). Short pitch cholesteric electro-optical device based on periodic polymer structures. *Applied Physics Letters*, 95, 011102–011104.
- Chigrinov, V., Kwok, H. S., Takada, H., & Takatsu, H. (2005). Photo-aligning by azo-dyes: Physics and applications. *Liquid Crystals Today*, 14, 1–15.
- Choi, S. S., Morris, S. M., Coles, H. J., & Huck, W. T. S. (2007). Wavelength tuning the photonic band gap in chiral nematic liquid crystals using electrically commanded surfaces. *Applied Physics Letters*, 91, 231110/1–3.
- Choi, S. S., Morris, S. M., Huck, W. T. S., & Coles, H. J. (2009a). The switching properties of chiral nematic liquid crystals using electrically commanded surfaces. *Soft Matter*, 5, 354–362.
- Choi, S. S., Morris, S. M., Huck, W. T. S., & Coles, H. J. (2009b). Electrically tuneable liquid crystal photonic bandgaps. *Advanced Materials*, 21, 3915–3918.
- Clark, N. A., & Lagerwall, S. T. (1980). Submicrosecond bistable electro-optic switching in liquid crystals. *Applied Physics Letters*, 36, 899–901.
- Crawford, G. (2003). Electrically Switchable Bragg Gratings. *Optics and Photonics News*, 14(4), 54–59.
- Cunningham, A., Mühlig, S., Rockstuhl, C., & Bürgi, T. (2011). Coupling of plasmon resonances in tunable layered arrays of gold nanoparticles. *Journal of Physical Chemistry C*, 115, 8955–8960.
- d'Alessandro, A., Donisi, D., De Sio, L., Beccherelli, R., Asquini, R., Caputo, R., et al. (2008). Tunable integrated optical filter made of a glass ion-exchanged waveguide and an electro-optic composite holographic grating. *Optics Express*, 16, 9254–9260.
- De Jeu, W. H., Gerritsma, C. J., Van Zanten, P., & Goossens, W. J. A. (1972). Relaxation of the dielectric constant and electrodynamic instabilities in a liquid crystal. *Physics Letters*, 39A, 355–356.
- De Sio, L., Caputo, R., De Luca, A., Veltri, A., & Umeton, C. (2006). In situ optical control and stabilization of the curing process of holographic gratings with a nematic film–polymer-slice sequence structure. *Applied Optics*, 45, 3721–3727.
- De Sio, L., Tabiryan, N., Caputo, R., Veltri, A., & Umeton, C. (2008). POLICRYPS structures as switchable optical phase modulators. *Optics Express*, 16, 7619–7624.
- De Sio, L., Serak, S., Tabiryan, N., Ferjani, S., Veltri, A., & Umeton, C. (2010). Composite holographic gratings containing light-responsive liquid crystals for visible bichromatic switching. *Advanced Materials*, 22(21), 2316–2319.
- De Sio, L., Tedesco, A., Tabiryan, N., & Umeton, C. (2010). Optically controlled holographic beam splitter. *Applied Physics Letters*, 97, 183507–183509.
- De Sio, L., Ferjani, S., Strangi, G., Umeton, C., & Bartolino, R. (2011). Universal soft matter template for photonic applications. *Soft Matter*, 7, 3739–3743.
- De Sio, L., Caputo, R., Cataldi, U., & Umeton, C. (2011). Broad band tuning of the plasmonic resonance of Gold nanoparticles hosted in self-organized soft materials. *Journal of Materials Chemistry*, 21, 18967.
- De Sio, L., Cunningham, A., Verrina, V., Tone, C. M., Caputo, R., Bürgi, T., et al. (2012). Double active control of the plasmonic resonance of a gold nanoparticle array. *Nanoscale*, 4, 7619–7623.
- Drzaic, P. S. (1995). *Liquid crystal dispersions* (pp. 30–59). Singapore: World Scientific.
- Feigenbaum, E., Diest, K., & Atwater, H. A. (2010). Unity-order index change in transparent conducting oxides at visible frequencies. *Nano Letters*, 10, 2111–2116.
- Gennes, P. G. D., & Prost, J. (1995). *The physics of liquid crystals* (2nd ed.). United Kingdom: Oxford University Press.
- Gerber, P. R. (1984). Two-frequency addressing of a cholesteric texture change electro-optical effect. *Applied Physics Letters*, 44, 932–934.

- Gilardi, G., De Sio, L., Beccherelli, R., Asquini, R., d'Alessandro, A., & Umeton, C. (2011). Observation of tunable optical filtering in photosensitive composite structures containing liquid crystals. *Optics Letters*, 36, 4755–4757.
- Guillard, H., Sixou, P., Reboul, L., & Perichaud, A. (2001). Electrooptical characterization of polymer stabilized cholesteric liquid crystals. *Polymer*, 42, 9753–9762.
- Hegde, G., & Komitov, L. (2010). Periodic anchoring condition for alignment of a short pitch cholesteric liquid crystal in uniform lying helix texture. *Applied Physics Letters*, 96, 113503–113505.
- Hikmet, R. A. M., & Kemperman, H. (1998). Electrically switchable mirrors and optical components made from liquid-crystal gels. *Nature*, 392, 476–479.
- Hikmet, R. A. M., & Kemperman, H. (1999). Switchable mirrors of chiral liquid crystal gels. *Liquid Crystals*, 26, 1645–1653.
- Hsiao, Y.-C., Tang, C.-Y., & Lee, W. (2011). Fast-switching bistable cholesteric intensity modulator. *Optics Express*, 19, 9744–9749.
- Hrozhyk, U., Serak, S., Tabiryan, N., & Bunning, T. J. (2006). Wide temperature range azobenzene nematic and smectic LC materials. *Molecular Crystals and Liquid Crystals*, 454, 235–245.
- Hrozhyk, U., Serak, S., Tabiryan, N., & Bunning, T. J. (2007). Photoinduced isotropic state of cholesteric liquid crystals: Novel dynamic photonic materials. *Advanced Materials*, 19, 3244–3247.
- Hrozhyk, U., Serak, S., Tabiryan, N., Hoke, L., Steeves, D. M., Kimball, B., et al. (2008). Systematic study of absorption spectra of donor-acceptor azobenzene mesogenic structures. *Molecular Crystals and Liquid Crystals*, 489, 257[583]–272 [598].
- Hrozhyk, U. A., Serak, S. V., Tabiryan, N. V., Hoke, L., Steeves, D. M., & Kimball, B. R. (2010). Azobenzene liquid crystalline materials for efficient optical switching with pulsed and/or continuous wave laser beams. *Optics Express*, 18(8), 8697–8704.
- Ishihara, S. (2005). How far has the molecular alignment of liquid crystals been elucidated? *IEEE/OSA Journal of Display Technology*, 1, 30–40.
- Johnson, P. B., & Christy, R. W. (1972). Optical constants of the noble metal. *Physical Reviews B*, 6, 4370–4379.
- Kinnan, M. K., & Chumanov, G. (2010). Plasmon coupling in two-dimensional arrays of silver nanoparticles: II. Effect of the particle size and interparticle distance. *Journal of Physical Chemistry C*, 114, 7496–7501.
- Kogelnik, H. (1969). Coupled wave theory for thick hologram gratings. *Bell System Technical Journal*, 48, 2909–2947.
- Kogelnik, H., & Shank, C. V. (1971). Simulated emission in a periodic structure. *Applied Physics Letters*, 18, 152–154.
- Klosterman, J., Natarajan, L., Tondiglia, V., Sutherland, R., White, T., Guymon, C., et al. (2004). The influence of surfactant in reflective HPDLC gratings. *Polymer*, 45, 7213.
- Kossyrev, P. A., Yin, A., Cloutier, S. G., Cardimona, D. A., Huang, D., Alsing, P. M., et al. (2005). Electric Field Tuning of Plasmonic Response of Nanodot Array in Liquid Crystal Matrix. *Nano Letters*, 5, 1978.
- Knoll, H. (2004). In W. Horspool, & F. Lenci (Eds.), *Organic photochemistry and photobiology. Photoisomerism of azobenzenes*. Boca Raton: CRC Press.
- Li, Z., Desai, P., Akins, R., Ventouris, G., & Voloschenko, D. (2002). Electrically tunable color for full-color reflective displays. *Proceedings of SPIE*, 4658, 7–13.
- Lin, T.-H., Jau, H.-C., Chen, C.-H., Chen, Y.-J., Wei, T.-H., & Chen, C.-W. (2006). Electrically controllable laser based on cholesteric liquid crystal with negative dielectric anisotropy. *Applied Physics Letters*, 88, 061122/1–3.
- Liu, Y., Sun, X., Dai, H., Liu, J., & Xu, K. (2005). Effect of surfactant on the electro-optical properties of holographic polymer dispersed liquid crystal Bragg gratings. *Optical Materials*, 27(8), 1451–1455.

- Liu, Y., & Sun, X. (2008). Holographic polymer-dispersed liquid crystals: Materials, formation, and applications. *Advanced Optics Electronics*, 2008(684349), 684341–684352.
- Liu, Q., Cui, Y., Gardner, D., Li, X., He, S., & Smalyukh, I. I. (2010). Self-alignment of plasmonic gold nanorods in reconfigurable anisotropic fluids for tunable bulk metamaterial applications. *Nano Letters*, 10, 1347–1353.
- Liu, Y. J., Hao, Q., Smalley, J. S. T., Liou, J., Khoo, I. C., & Huang, T. J. (2010b). A frequency-addressed plasmonic switch based on dual-frequency liquid crystals. *Applied Physics Letters*, 97, 091101.
- Link, S., & El-Sayed, M. A. (1999). Size and temperature dependence of the plasmon absorption of colloidal gold nanoparticles. *Journal of Physical Chemistry B*, 103, 4212–4217.
- Lu, S.-Y. & Chien, L.-C. (2007). A polymer-stabilized single-layer color cholesteric liquid crystal display with anisotropic reflection. *Applied Physics Letters*, 91, 131119/1–3.
- Meng, S., Kyu, T., Natarajan, L., Tondiglia, V., Sutherland, R., & Bunning, T. (2005). Holographic photo-polymerization induced phase separation in reference to the phase diagram of a mixture of photo-curable monomer and nematic liquid crystal. *Macromolecules*, 38, 4844–4854.
- Meyer, R. B. (1968). Effects of electric and magnetic fields on the structure of cholesteric liquid crystals. *Applied Physics Letters*, 12, 281–282.
- Meyer, R. B. (1969). Piezoelectric effects in liquid crystals. *Physical Review Letters*, 22, 918–921.
- Mie, G. (1908). Beitrage zur Optik truber Medien speziell kolloidaler Metallosungen. *Annals of Physics*, 25, 377–445.
- Montemezzani, G., & Zgonik, M. (1997). Light diffraction at mixed phase and absorption gratings in anisotropic media for arbitrary geometries. *Physical Review E*, 55(1), 1035–1047.
- Natarajan, L., Sutherland, R., Tondiglia, V., Bunning, T., & Adams, W. (1996). Electro-optical switching characteristics of volume holograms in polymer dispersed liquid crystals. *Journal of Nonlinear Optical Physics and Materials*, 5(1), 89–98.
- Natarajan, L., Brown, D., Wofford, J., Tondiglia, V., Sutherland, R., Lloyd, P., et al. (2006). Holographic polymer dispersed liquid crystal reflection gratings formed by visible light initiated thiol-ene photopolymerization. *Polymer*, 47(12), 4411–4420.
- Natarajan, L. V., Wofford, J. M., Tondiglia, V. P., Sutherland, R. L., Koerner, H., & Vaia, R. A. (2008). Electro-thermal tuning in a negative dielectric cholesteric liquid crystal material. *Journal of Applied Physics*, 103, 093107/1–6.
- Natarajan, L. V., Wofford, J. M., Tondiglia, V. P., Sutherland, R. L., Siwecki, S. A., & Koerner, H. (2007). Tuning of a cholesteric filter having a negative dielectric anisotropy. *Proceedings of SPIE*, 6654, 66540A/1–6.
- Nersisyan, S. R., Tabiryan, N. V., Steeves, D. M., & Kimball, B. (2009). Optical axis gratings in liquid crystals and their use for polarization insensitive optical switching. *Journal of Nonlinear Optical Physics and Materials*, 18(1), 1–47.
- Nersisyan, S. R., Kimball, B. R., Steeves, D. M., & Tabiryan, N. V. (2010). Technology of diffractive waveplates for polarizer-free displays. *IMID/IDMC/ASIA Display Digest*, 277–278.
- Patel, J. S., & Meyer, R. B. (1987). Flexoelectric electro-optics of a cholesteric liquid crystal. *Physical Review Letters*, 58, 1538–1540.
- Pogue, R., Natarajan, L., Siwecki, S., Tondiglia, V., Sutherland, R., & Bunning, T. (2000). Monomer functionality effects in the anisotropic phase separation of liquid crystals. *Polymer*, 41(2), 733–741.
- Ren, H., & Wu, S.-T. (2002). Reflective reversed-mode polymer stabilized cholesteric texture light switches. *Journal of Applied Physics*, 92(2), 797–800.



- Sathaye, K. S., Dupont, L., & de Bougrenet de la Tocnaye, J.-L. (2012). Asymmetric tunable Fabry-Perot cavity using switchable polymer stabilized cholesteric liquid crystal optical Bragg mirror. *Optical Engineering*, 51, 034001/1–7.
- Schulte, M., Clarson, S., Natarajan, L., Tomlin, D., & Bunning, T. (2000). The effect of fluorine-substituted acrylate monomers on the electro-optical and morphological properties of polymer dispersed liquid crystals. *Liquid Crystals*, 27(4), 467–475.
- Senyurt, A., Warren, G., Whitehead, J., & Hoyle, C. (2006). Matrix physical structure effect on the electro-optic characteristics of thiol-ene based H-PDLC films. *Polymer*, 47(8), 2741–2749.
- Serak, S., & Tabiryan, N. (2006). Microwatt power optically controlled spatial solitons in azobenzene liquid crystals. *SPIE Proceedings*, 6332, 63320Y1–63320Y13.
- Serak, S. V., Tabiryan, N. V., & Bunning, T. J. (2007). Nonlinear transmission of photosensitive cholesteric liquid crystals due to spectral bandwidth auto-tuning or restoration. *Journal of Nonlinear Optical Physics and Materials*, 16, 471–483.
- Strangi, G., Barna, V., Caputo, R., De Luca, A., Versace, C., Scaramuzza, N., et al. (2005). Color-tunable organic microcavity laser array using distributed feedback. *Physical Review Letters*, 94, 063903–063906.
- Sutherland, R. (2002). Polarization and switching properties of holographic polymer-dispersed liquid-crystal gratings. I. Theoretical model. *Journal of the Optical Society of America B*, 19(12), 2995–3003.
- Tabiryan, N., Hrozhyk, U., & Serak, S. (2004). Nonlinear refraction in photoinduced isotropic state of liquid crystalline azobenzenes. *Physical Review Letter*, 93, 113901(1)–113901(4).
- Tabiryan, N., Nersisyan, S. R., Steeves, D. M., & Kimball B. R. (2010). The promise of diffractive waveplates. *Optics and Photonics News*, 21(3), 41–45.
- Tondiglia, V. T., Natarajan, L. V., Bailey, C. A., Duning, M. M., Sutherland, R. L., & Yang, D.-K. (2011). Electrically induced bandwidth broadening in polymer stabilized cholesteric liquid crystals. *Journal of Applied Physics*, 110, 053109/1–8.
- Urbas, A., Beckel, E., Tondiglia, V., Natarajan, L., & Bunning, T. (2006). Holographic liquid crystal photonic materials stabilized with monoacrylate LC monomer. *American Physical Society*, W28.009.
- Vaia, R., Tomlin, D., Schulte, M., & Bunning, T. (2001). Two-phase nanoscale morphology of polymer/LC composites. *Polymer*, 42, 1055.
- Veltri, A., Caputo, R., Umeton, C., & Sukhov, A. V. (2004). Model for the photoinduced formation of diffraction gratings in liquid-crystalline composite materials. *Applied Physics Letters*, 84, 3492–3494.
- Wendorff, J. H. (2006). Holographic storage via the liquid crystal state: a success story. *Liquid Crystals*, 33, 1419–1420.
- White, T. J., Bricker, R. L., Natarajan, V., Serak, S., Tabiryan, N., & Bunning, T. J. (2009). Polymer stabilization of phototunable cholesteric liquid crystals. *Soft Matter*, 5, 3623–3628.
- Wu, S. T., Efron, U., & Hess, L. D. (1984). Birefringence measurements of liquid crystals. *Applied Optics*, 23, 3911–3915.
- Xianyu, H., Faris, S., & Crawford, G. P. (2004). In-plane switching of cholesteric liquid crystals for visible and near-infrared applications. *Applied Optics*, 43, 5006–5015.
- Xu, M., & Yang, D.-K. (1997). Dual frequency cholesteric light shutters. *Applied Physics Letters*, 70, 720–722.
- Yeh, P., & Gu, C. (1999). *Optics of liquid crystal displays* (pp. 282–305). New York: Wiley.
- Yu, H., Tang, B. Y., Li, J., & Li, L. (2005). Electrically tunable lasers made from electro-optically active photonics band gap materials. *Optics Express*, 13, 7243–7249.